Aus dem

Zentrum für Neurodynamik und Magnetoenzephalographie
Hertie-Institut für klinische Hirnforschung
Universität Tübingen

Comparison of electrical and pneumatic somatosensory evoked fields - A MEG Study

Inaugural-Dissertation
zur Erlangung des Doktorgrades
der Medizin

der Medizinischen Fakultät
der Eberhard Karls Universität
zu Tübingen

vorgelegt von

Li, Siyu

2025

Dekan: Professor Dr. B. Pichler

1. Berichterstatter: PD Dr. J. Marquetand
2. Berichterstatter: PD Dr. T. Rattay

Tag der Disputation: 28.02.2025

Table of Contents：

List of all figures:

List of all tables:

List of abbreviations:

AP	Action potential
BOLD	Blood level-dependent
EEG	Electroencephalography
EM	Electrical stimulation of the median nerve
ERF	Event-related field
ERP	Event-related potential
ET	Electrical stimulation of the tibial nerve
fMRI	Functional magnetic resonance imaging
fT	Femtotesla
Fig	Figure
GMFP	Global mean field power
ICA	Independent component analysis
MEG	Magnetoencephalography
mm	Millimeter
ms	Millisecond
MSR	Magnetically shield room
PM	Pneumatic stimulation of the median nerve
PSP	Post-synaptic potential
PT	Pneumatic stimulation of the tibial nerve
SD	Standard deviation
SEF	Somatosensory evoked field
SEP	Somatosensory evoked potential
SI	Primary somatosensory cortex
SII	Secondary somatosensory cortex
SQUID	Superconducting quantum interference devices
T	Tesla

1. Introduction

1.1 Human somatosensory system

The human somatosensory system is a neural network that processes sensations of touch, pressure, temperature, pain, and proprioception (i.e., sensations of body position and movement). This system enables humans to perceive changes in both internal and external environments and respond accordingly(Purves et al., 2019, Abraira et al., 2013).

Tactile perception is central to our research. Early studies used electrical stimulation to simulate tactile sensations and generate clear somatosensory evoked potentials (SEP) and fields (SEF), enhancing our understanding of neural pathways and processes. However, electrical stimulation often causes discomfort in participants, as it stimulates not only tactile but also pain and motor fibers. Recent studies have explored pneumatic stimulation to better mimic natural touch. Nevertheless, SEP or SEF from pneumatic stimulation typically exhibit less distinct characteristics than those from electrical stimulation, prompting an investigation into how the brain processes these stimuli differently(Nakamura et al., 1998, Antonakakis et al., 2019, Bromm et al., 1998).

This study compared SEF under electrical and pneumatic stimulation conditions, focusing on the axial and planar topography of the M20 and M37 components. We aimed to reveal the brain's responses to different types of tactile stimuli. This chapter will introduce fundamental concepts related to the somatosensory system, SEP, and magnetoencephalography (MEG), all essential for understanding this study.

1.1.1 Somatosensory pathways

In this study, we activated the somatosensory pathway using electrical and pneumatic stimulation, focusing exclusively on non-painful tactile stimulation.

Non-painful tactile stimulation primarily follows the medial lemniscus pathway. Receptors in the skin, muscles, and joints convert these stimuli into neural signals. These signals propagate via peripheral nerves to the posterior horn of the spinal cord (Cruccu et al., 2008, Kaas, 2004). After reaching the posterior horn, somatosensory input ascends to the ipsilateral cuneate nucleus in the lower brainstem. Here, the input crosses to the contralateral side of the body before ascending to the thalamus and projecting to the primary somatosensory cortex (SI) **(Figure 1)**(Kaas, 2004, Cruccu et al., 2008)**.**

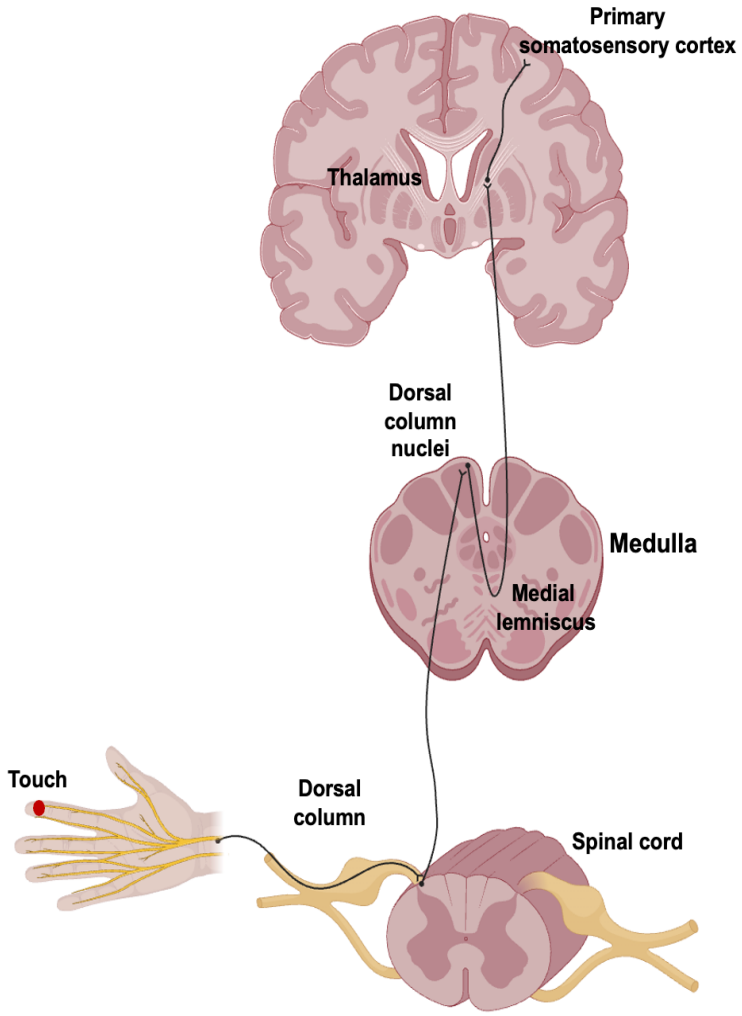

Figure 1. The somatosensory pathway from peripheral receptors to the cerebral cortex is the medial lemniscus (black line). This figure was made according to (Cruccu et al., 2008) and created with Biorender.com.

1.1.2 Somatosensory cortex

In the human somatosensory system, the processing of tactile input involves a complex process across multiple regions of the brain's cortex. The SI, located between the central sulcus and postcentral gyrus, is the initial site where tactile signals reach the somatosensory cortex. Anatomically, SI can be divided into four subregions according to the Brodmann map: 3a, 3b, 1, and 2 **(Figure 2)**, each with distinct functions in the processing of somatosensory signals(Kaas, 2004, Kallio, 2018).

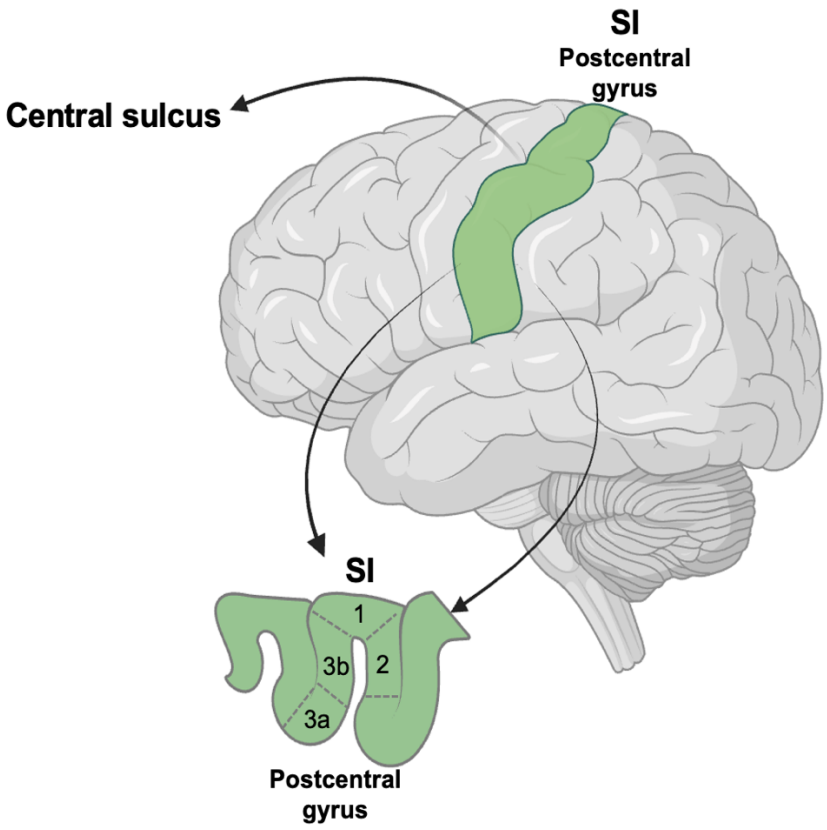

Figure 2. Anatomy of somatosensory cortex SI (green area). SI region is divided into four sub-regions: 3a, 3b, 1, and 2. This figure was made according to (Purves, 2018) and created with Biorender.com.

When tactile signals enter the SI from the thalamus, they first reach Brodmann area 3b. This area, located in the rostral part of the postcentral gyrus, directly receives tactile signals from various parts of the body and performs initial

processing of signal intensity, timing, and frequency. Area 3a, adjacent to area 3b, integrates somatosensory and motor signals to control and coordinate body movements(Kaas, 2004). Areas 1 and 2 engage in higher-level processing of tactile properties, such as object texture, hardness, and shape. Additionally, area 2 is responsible for spatial perception and motor control functions, regulating body posture and movement in space. Notably, the functional representation within the SI regions is not entirely independent but involves some overlap. The interaction among these subregions enables SI to process somatosensory information thoroughly, thereby providing refined perceptual abilities.

The primary somatosensory cortex (SI) is the initial station for processing tactile basic properties such as intensity, location, and texture. This thesis focuses on the differences in how stimuli are processed within the SI region, particularly through M20 and M37, which are commonly studied components of somatosensory evoked fields (SEF). The next chapter will introduce the basics of SEF and its application to tactile signal processing.

1.2 Somatosensory evoked fields

1.2.1 Somatosensory evoked fields

In the resting state, the brain spontaneously generates periodic neural oscillations that regulate essential physiological functions. Following an external stimulation or a task, the brain generates specific evoked responses, which can be studied and recorded using event-related potentials or fields (ERP or ERF). ERP or ERF is typically detected through EEG or MEG, widely utilized in neuroscience research. This study focuses on somatosensory evoked potentials/fields (SEP/SEF), a subset of ERP/ERF. SEP is commonly used in clinical neurophysiology to assess the somatosensory system's conduction velocity and pathway integrity, helping diagnose neurological disorders(Kallio, 2018, Leonardelli, 2010).

1.2.2 SEF components

SEF can be recorded following stimulation of various body parts,allowing us to examine the brain response of different somatosensory pathways. The median and tibial nerves represent the somatosensory pathways of the upper and lower limbs, respectively. After stimulation of these nerves, these somatosensory signals typically propagate along their respective somatosensory pathway to specific regions of the SI **(Figure 3A)**(Buchner et al., 1994, Kakigi et al., 1995).

Following stimulation of the median or tibial nerve, the M20 or M37 component of the magnetic brain activity emerges around at 20 ms and 37 ms post-stimulation, respectively **(Figure 3B and 3C).** These waveforms reflect the initial processing of somatosensory stimulation in area 3b of SI(Beppi et al., 2021, Leonardelli, 2010, Anzellotti et al., 2016). The latency of M37 is notably more prolonged than that of the M20 component following median nerve stimulation due to the longer distance of the lower limb from the SI. The short-latency components, such as M20, typically serve as objective measures for assessing somatosensory function and diagnosing various neurological conditions(Tecchio et al., 2007)**.** For instance, the latency of M20 or M37 indicates the speed of neural conduction, with prolonged latencies suggesting potential damagess in the somatosensory system. This makes them valuable for identifying conditions such as peripheral neuropathy, or spinal cord injury, where delayed signal transmission is common(Hitomi et al., 2006, Walsh et al., 2005). In addition to latency, the amplitude of M20 or M37 always represents the degree of cortical activation in response to sensory stimuli. Reduced amplitudes may indicate impaired cortical processing or diminished somatosensory input, as seen in stroke or neurodegenerative diseases. Conversely, increased amplitudes may suggest cortical hyperexcitability, which is often associated with disorders such as epilepsy(Ostry et al., 2021, Assenza et al., 2020).In contrast to the rapid response

of SI, secondary somatosensory cortex (SII) exhibits a delayed response to somatosensory stimuli, typically occurring between 95 and 125 ms post-stimulation after median nerve stimulation(Hari et al., 1984). This time difference suggests that SI mainly processes primary tactile information, while SII may be involved in higher-level sensory integration and processing.

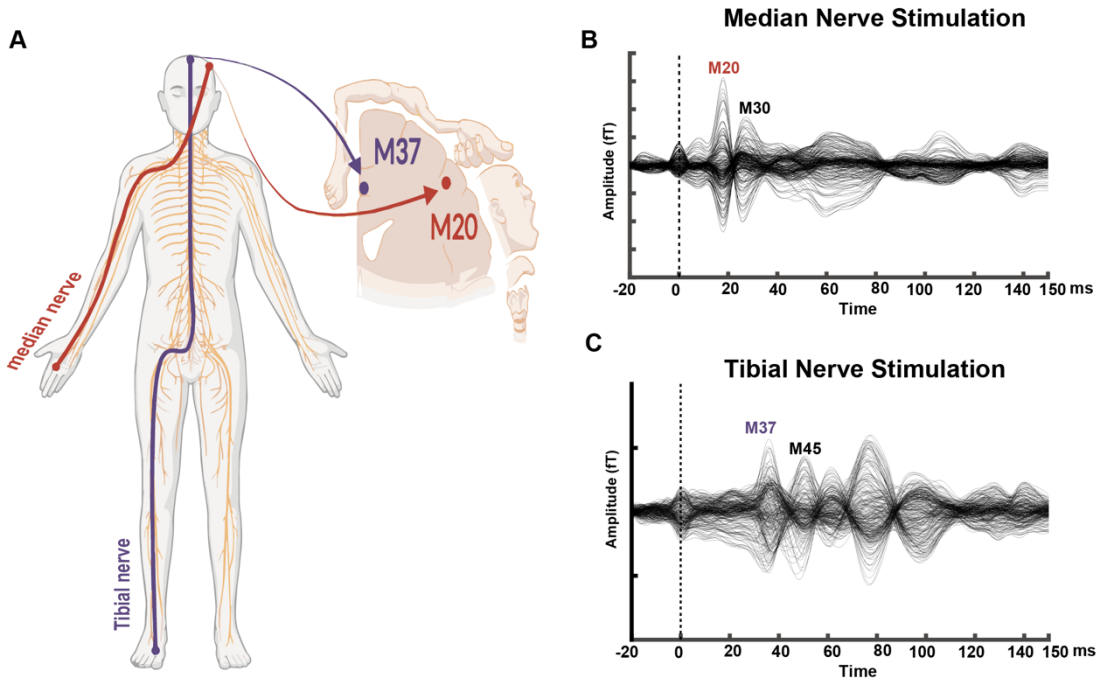

Figure 3. SEF conduction pathways and waveforms; (A) Conduction pathways of SEF from the median (red line) or tibial nerve (purple line) to specific SI regions; (B) Waveforms of SEF following median nerve stimulation, including M20 and M30 components; (C) Waveforms of SEF following tibial nerve stimulation, including M37 and M45 components. The dotted line in (B) and (C) indicates the stimulation artifact.The Fig. 3A was made according to (Maudrich et al., 2021) and (Levin et al., 2019) and created with Biorender.com.

1.2.3 Stimulation types of SEF

The somatosensory system is frequently stimulated by applying electrical or mechanical peripheral somatosensory stimulation. This study utilized both electrical stimulation and pneumatically-driven mechanical stimulation. Electrical stimulation involves applying electrical current to nerves, which triggers excitatory responses in the somatosensory system. These neural excitations propagate along the somatosensory pathway to the SI region, generating a sensation to be

felt specifically at the stimulation area. On the other hand, pneumatic stimulation uses a pneumatic pump to deliver compressed air through a hose to activate mechanoreceptors in the skin. Action potentials generated by these mechanoreceptors are transmitted to peripheral nerve fibers and then to the brain cortex, particularly the SI region. While both stimulation modes produce similar SI responses(Mertens et al., 2000), they exhibit significant differences in signal-to-noise ratio(SNR).

Electrical stimulation activates numerous nerve fibers, generating the high SNR SEP or SEF signal, commonly used in clinical neurophysiological testing(Leonardelli, 2010). These clear signals are particularly important for precisely measuring latencies in SEP or SEF components, such as diagnosing delayed neural processing indicative of multiple sclerosis(Kallmann et al., 2006). Additionally, electrical stimulation can modulate specific pain fibers, like Aδ fibers that transmit sharp, localized pain and C fibers responsible for dull, throbbing pain, making it a useful tool in pain research(Torebjork et al., 1980).In contrast, pneumatic stimulation is gentler , producing blurred signals with a lower signal-to-noise ratio. Due to its mild stimulation method, pneumatic stimulation typically does not cause discomfort to participants, making it suitable for prolonged experimental studies or sensitive participants, such as children. Pneumatic stimulation is used to simulate natural tactile experiences and study tactile mechanisms, including the activation of skin mechanoreceptors(Nakamura et al., 1998, Lew et al., 2009, Onishi et al., 2013).

Nowadays, many studies have separately explored SEF characteristics under electrical and pneumatic stimulation conditions, but there are few direct comparative studies on the topographic representations This study compared the axial and planar topography of SEF components M20 and M37 under electrical

and pneumatic stimulation to reveal how the brain processes different tactile stimuli. MEG is used to achieve this goal in this study and is known for its high spatial and temporal resolution. The following sections outline MEG's history, fundamental principles, and applications in neuroimaging.

1.3 MEG

1.3.1 MEG history

Magnetoencephalography (MEG) is a non-invasive neuroimaging device that detects weak magnetic fields generated by electrical currents within the brain(Babiloni et al., 2009). Originally measured by Cohen in 1968 using a copper induction coil, MEG signals were of poor quality with a low signal-to-noise ratio. The copper coil's sensitivity to brain magnetic fields is low because it relies on electromagnetic induction, which requires a substantial change in magnetic flux to produce a detectable voltage. Brain magnetic fields are often too small to induce a strong current in the copper coil (Cohen, 1968). In 1972, the Superconducting Quantum Interference Device (SQUID) was introduced as a magnetic detector, greatly enhancing MEG's sensitivity to small biomagnetic fields. Initially, only one SQUID detector was used, requiring constant repositioning to measure the magnetic fields around the subject's head(Cohen, 1972). Since 1980, MEG has utilized multiple sensors covering a large area of the head to measure signals simultaneously(Hämäläinen et al., 1993). In 1992, the first helmet-mounted MEG device was introduced with 148 channels to cover most of the head(Vrba et al., 2001). Presently, MEG systems have 100-300 channels covering almost the whole head(Fred et al., 2022). Therefore, MEG signals can be efficiently collected with millisecond (ms) temporal and millimeter (mm) spatial resolutions(Hämäläinen et al., 1993).

1.3.2 MEG system

Biomagnetism involves measuring the weak magnetic fields generated by neural and muscular activity(Williamson et al., 2013). Among these, the strongest

biomagnetic signal produced by the human body is the cardiac magnetic field, recorded using magnetocardiography (Zhu et al., 2022).The magnetic field generated by the human brain is extremely weak, approximately 10^{-13} to 10^{-14} Tesla (T). Electrical devices and the earth's magnetic field are classified as external magnetic fields.These fields are generated by the electrical activity from natural or man-made sources.However, external magnetic fields are much higher than the brain's magnetic field. For instance, the earth's magnetic field is around 10^{-4} T, approximately a billion times stronger than the brain's **(Figure 4)** (Vrba, 2002). These external magnetic fields can interfere with the measurement of weak biomagnetic fields,making accurate detection of the brain’s magnetic field a significant challenge. Consequently, specialized magnetic shielding and advanced techniques are essential to easure precise recording in brain magnetic field experiments.

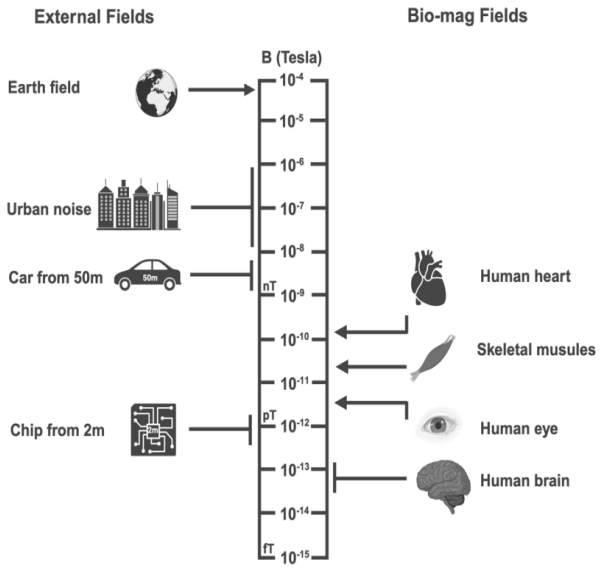

Figure 4. Comparison of the biomagnetic fields with other external fields. This figure was made according to (Vrba, 2002) and created with Biorender.com

Several key components are used for the MEG system to increase magnetic field sensitivity and minimize external interference, such as the magnetically shielded

room (MSR), SQUID, and Dewar **(Figure 5)**. Here, I will briefly describe these key components.

MSR: The MEG is typically placed within a magnetically shielded room (MSR) to eliminate interference from household appliances or the earth's magnetic field, ensuring the reliability of the measured neural signals. The MSR usually has a middle layer of aluminum coated with copper, which provides good mechanical strength and electrical conductivity, effectively blocking changing magnetic fields by generating eddy currents. However, this middle layer does not shield against static magnetic fields. The outer and inner layers are made of mu-metal, with high magnetic susceptibility. These two layers attract and guide external magnetic fields around the measurement site, thus enhancing the shielding effectiveness against external disturbances (Holmes et al., 2022).

SQUID: Besides mitigating interference from external magnetic fields, enhancing the MEG's sensitivity to weak biomagnetic fields is another challenge. The SQUID, the most sensitive magnetic flux detector, serves as a critical component of the MEG system. Its principal structure, the Josephson junction, converts minute magnetic flux changes into electrical currents In general, the sensitivity of SQUID detectors in MEG typically ranges between 2-3 fT/$\sqrt{Hz}$, which is adequate for effectively recording the brain's magnetic fields(Cohen, 1972, Faley et al., 2006).

Dewar: The sensors of MEG must be maintained in a superconducting state, housed within a helmet-like container known as a Dewar. The interior of the Dewar is filled with liquid helium, which cools the SQUID coils below 4.2 K, sustaining its superconducting state for highly sensitive magnetic field detection. Typically constructed from double glass or metal, the Dewar utilizes a vacuum to seal the space between the double layers, minimizing heat conduction from the subject's head temperature (close to body temperature) to the sensor (required

to remain below 4.2 K) (Niso Galán, 2013).

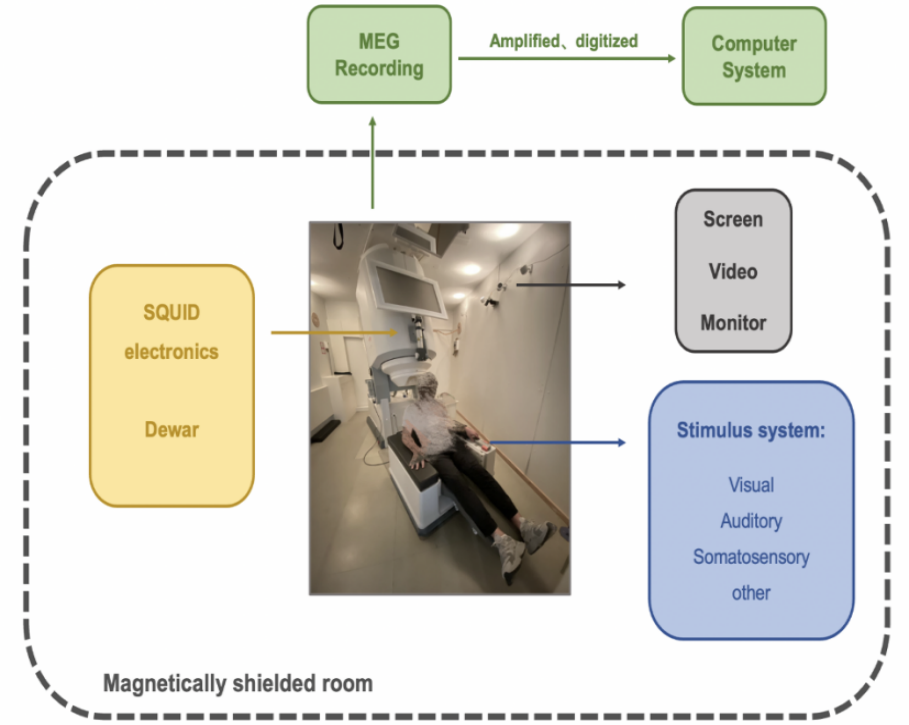

Figure 5. Schematic diagram of the MEG device. Typically, the MEG measurement process involves subjects engaging in tasks related to the study topic, such as responding to visual, auditory, or tactile stimulation. During these tasks, the SQUID coil records the brain's magnetic field signals simultaneously. These signals are then captured, amplified, digitized, and transferred to a computer system for storage, processing, and analysis. This figure was made according to (Vrba et al., 2001) and created with Biorender.com.

1.3.3 Origin of MEG signals

The human brain is a complex neural network consisting of approximately 10^{11} neurons, each interconnected by about 10^3 synapses facilitating neural signal transmission. These signals propagate through electrical and chemical means. Specifically, signal transmission along neuron axons is mediated by action potentials (AP), rapid and transient electrical signals arising from the opening and closing of ion channels on the neuron membrane. This process mainly involves the efflux of potassium ions and the influx of sodium ions, lasting approximately 1 ms. When AP reaches the synapse at the end of the axon, it initiates the release of excitatory or inhibitory neurotransmitters into the synaptic cleft. Subsequently,

these neurotransmitters bind to receptors on the postsynaptic membrane, activating channels such as those for calcium ions, thus altering the membrane potential and generating postsynaptic potentials (PSP) spanning approximately 10 ms **(Figure 6)** (Niso Galán, 2013, Pakkenberg et al., 2003).

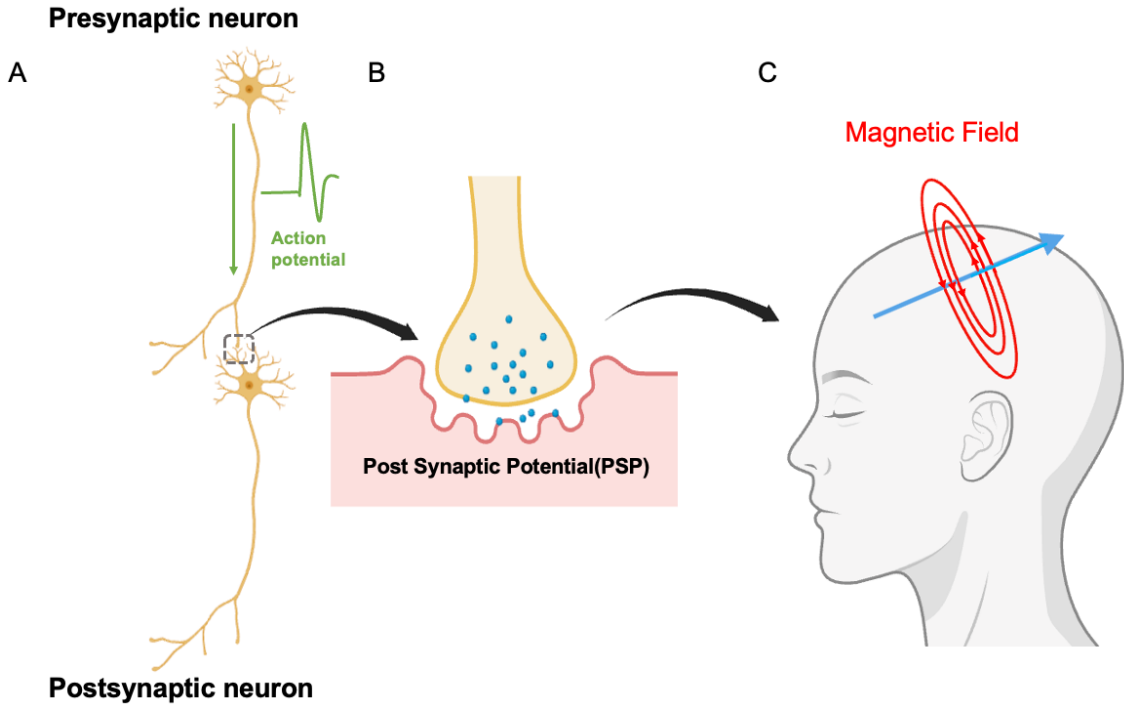

Figure 6. Origin of neural signals measured by MEG; (A) Action potential transmission process along the axon of the pre-synaptic neuron (green arrow); (B) Post-synaptic potential generated by neurotransmitters (blue dots) binding to ionotropic receptors on the postsynaptic membrane; (C) Magnetic field (red circle and arrow) generated by the current associated with the postsynaptic potential (blue arrow); This figure was made according to (Vrba et al., 2001) and created with Biorender.com.

Based on Maxwell's equations, the activation of neurons at their postsynaptic membrane generates weak electrical currents, inducing small magnetic fields spreading in circular patterns around the current.According to the right-hand rule, if the thumb of the right hand points in the direction of the current, the fingers will bend in the direction of the induced magnetic field. MEG can detect these field changes. While both PSP and AP can prompt magnetic field changes, MEG captures signals originating from the currents associated with PSP rather than

those linked to APs. The reasons for this are as follows(Niso Galán, 2013, Meyer, 2016):

1.) AP exhibits biphasic properties, with both positive and negative deflections. During depolarization, sodium ions are at the site, causing currents to travel in both directions. This bidirectional current flow results in the magnetic fields of both currents canceling each other to some extent, potentially reducing the overall signal strength. The signal propagates predominantly in the forward direction because the backward direction remains refractory. In contrast, PSP displays a monophasic nature, allowing for these potentials to accumulate and result in a stronger overall signal. At the apical dendrites, the current travels in a single direction, enhancing the detectability of these signals. As a result, MEG can detect PSP more efficiently than AP.
2.) The duration of PSP is approximately 10 ms, much longer than that of AP, which typically lasts about 1 ms. This longer duration allows for the temporal summation of PSP from multiple neurons and provides MEG with a broader time window to capture signals effectively.
3.) Generally, PSP generates an electric dipole with a circular magnetic field changing slowly in time (between 4 and 100 Hz). Conversely, AP involves a rapid depolarization and repolarization process, where depolarizing and repolarizing currents on axons move in both directions. These opposing currents lead to the cancellation of the magnetic fields generated. The decay rate of bipolar magnetic fields associated with PSP is much slower than that of quadrupolar fields linked to AP, especially at the apical dendrites, rendering PSP-related magnetic fields more readily detectable by MEG.

1.3.4 MEG vs. other techniques

MEG vs. EEG: Electroencephalography (EEG) and magnetoencephalography (MEG) measure scalp electrical potentials and magnetic fields generated by

electrical brain activity, respectively. While both modalities record signals from the electrical activity of parallel-aligned pyramidal neurons in the cerebral cortex, they exhibit differences(van Mierlo et al., 2019, Baillet, 2017, Hämäläinen et al., 1994, Henry, 2006):

1.) MEG shares a similar temporal resolution with EEG but offers higher spatial resolution due to the magnetic field's reduced susceptibility to scalp and skull conductivity changes, which minimizes interference from volumetric currents and artifacts.
2.) EEG is sensitive to radial and tangential signals, whereas MEG is only sensitive to tangential signals within the cortex. Because tangential currents (parallel to the scalp) produce magnetic fields that extend outside the head, making them detectable by MEG. However, radial currents (perpendicular to the scalp) generate magnetic fields that remain confined within the head, making them undetectable.
3.) The high cost of MEG's core components, such as liquid helium and MSR, has limited its widespread adoption. In comparison, EEG, which is relatively inexpensive, has been used in clinical settings for a longer period.

Despite these differences, more and more studies have demonstrated that MEG and EEG could complement each other rather than compete. Many MEG centers conduct EEG/MEG studies to explore brain function, particularly in investigating functional brain connectivity and elucidating mechanisms of some diseases, such as epileptic networks.

MEG vs fMRI: Functional Magnetic Resonance Imaging (fMRI) primarily detects hemodynamic changes in the brain, measured using blood oxygen level-dependent (BOLD) contrast. The main distinction between the two techniques is

that MEG offers higher temporal resolution at the millisecond level and can directly measure the brain's neuroelectric activity. While fMRI has a high spatial resolution, its temporal resolution is limited to seconds (Cargnelutti et al., 2023). Each technique has its advantages and limitations. Regarding resolution, the two techniques are complementary, and their combined use provides a comprehensive and reliable understanding of brain activity.

1.4 Aims and hypotheses

The overall aim objective of this study is to compare the waveform characteristics and topography of SEF under electrical and pneumatic stimulation. Since electrical stimulation often causes discomfort during clinical SEP or SEF testing, this study aims to explore whether pneumatic stimulation can serve as a viable alternative. The specific objectives of the study include:1.) Investigating whether there is a significant difference in the latencies of M20 and M37 between electrical and pneumatic stimulation; 2.)Assessing the signal-to-noise ratio (SNR) differences between the two stimulation methods; 3.) Analyzing the axial and planar topographies of M20 and M37 under both electrical and pneumatic stimulation to evaluate their differences and correlations

Hypothesis 1: Electrical stimulation will generate clearer and sharper M20 and M37 waveforms compared to pneumatic stimulation. This is attributed to the higher signal-to-noise ratio and quicker conduction path of electrical stimulation compared to pneumatic stimulation.

Hypothesis 2: After normalizing stimulus intensity, the topographic patterns of M20 and M37 under both electrical and pneumatic stimulation conditions will exhibit significant differences. These differences may stem from the involvement of different neural generators.

Hypothesis 3: Following normalization of stimulus intensity, there will be no significant correlation in the topography of SEF components M20 and M37 between electrical and pneumatic stimulation conditions. The different neural generators are involved into these two stimulations, no correlation should be present.

Hypothesis 4: Significant differences in the latency of M20 and M37 components are expected between electrical and pneumatic stimulation conditions. Specifically, we anticipate shorter latencies for M20 and M37 under electrical stimulation due to faster conduction paths, while pneumatic stimulation involves mechanical delays affecting SEF transmission.

2 Methods

2.1 Participants

Ten healthy participants were recruited from the University of Tübingen. All participants were right-handed and confirmed free of neurological disorders by a a senior neurologist. Before the measurements, all participants were informed to dress in metal-free clothes and provide written informed consent. The study complied with the Declaration of Helsinki and was approved by the University of Tübingen Ethics Committee (20V2023B0). The demographic characteristics of all participants are presented in Table 1 in the RESULTS section.

2.2 Experimental protocols

The study employed four different experimental setups for SEF, utilizing two stimulation methods (electrical and pneumatic) targeting two anatomical sites (median and tibial nerves). This section depicts the details of the experimental configuration (Figure 7).

1.) Electrical stimulation: It was administered to the right median nerve at the wrist (EM stimulation) and the right tibial nerve at the inner ankle, respectively (ET stimulation). Electrodes were positioned approximately 2 cm along the nerve projection direction **(Figure 7A and 7C).** Square wave pulses lasting 0.1 ms, with an interval of 300 ms, were delivered to evoke responses in the median or tibial nerve. Gradually increase the stimulation intensity until a slight twitching of the thumb (median nerve) or toe (tibial nerve) is observed without causing pain. This protocol ensured precise and controlled stimulation for both median and tibial nerves.
2.) Pneumatic stimulation: This method involves a balloon diaphragm operated by compressed air **(Figures 7B and 7D)**. For the right median nerve (PM stimulation), the stimulator was affixed to the right index finger, while for the right tibial nerve (PT stimulation), it was attached to the right toe. A

compressor outside the shielded room delivered air pulses through a sealed tube. These pulses lasted also 5 ms. An electronic trigger was sent to the recording computer whenever the valve opened to provide an air pulseer. Subsequent stimuli were spaced by intervals ranging between 250-350 ms. Stimuli were delivered at an intensity of 2000 Hektopascal. Due to the dynamics of air transfer through the tube, a delay of 40 milliseconds was observed in the pulses.

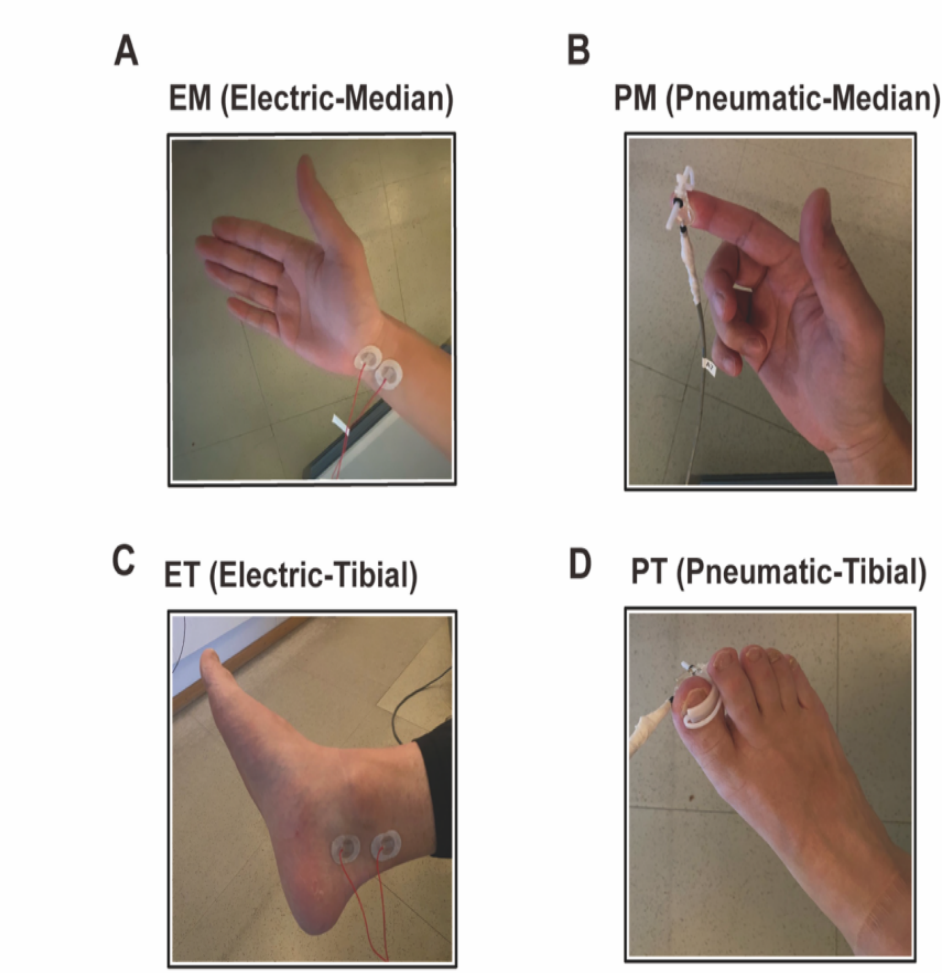

Figure 7. The stimulation types. (A)(C) Electrical stimulation was applied to the median (EM) or tibial (ET) nerve using square-wave electrical impulses until the thumb or toe twitched without causing pain. (C)(D) Pneumatic stimulation was delivered by a stream of compressed air to the index finger (median nerve, PM) and the toe (tibial nerve, PT) for tactile stimulation.

2.3 MEG data acquisition

In the magnetically shielded room, all participants sat upright in a chair for the measurements. Data were acquired using a 275-channel whole-head MEG system (CTF Inc., Vancouver, Canada) at a sampling rate of 2400 Hz. A built-in third-order gradiometer correction was applied to minimize external interference. Before data acquisition, three head position indicator coils were strategically placed at the nasion and left and right preauricular points (the position of three fiducial points) in order to determine the position of the head with respect to the sensor coils, and to ensure that head movements were accurately tracked throughout the recording.

Participants were instructed to keep their eyes closed and stay quiet throughout the procedure to reduce artifacts from eye blinking and muscle movements. Each experimental condition was administered for approximately 5 minutes. Approximately 1200 valid trials were finally acquired for each condition and participant during this period.

2.4 Pre-processing of MEG data

The MEG data was analyzed through MATLAB (version: R_2023b, the MathWorks, Inc.) and the neural signal processing toolkit Fieldtrip (https://www.fieldtriptoolbox.org). Each recording was visually inspected to identify and discard the channels or trials with significant artifacts, such as muscle contractions and sensor jumps. The continuous data were high-pass filtered at 2 Hz to remove slow drift, and a Notch filter was used to remove l 50 Hz line noise (and the harmonics at 100 and 150 Hz). Independent Component Analysis (ICA) was performed to remove artifacts resulting from heartbeats and eye movements, and eye blinks. Afterwards, the data were re-segmented into trials (according to recorded trigger information) with a duration of 70 ms for subsequent analysis, including a baseline of 20 ms pre-stimulation and data of 50 ms post-stimulation.

2.5 Somatosensory evoked fields

To improve the signal-to-noise ratio (SNR) of the somatosensory evoked fields (SEF), data were averaged across trials for each condition, with baseline correction from -20 ms to 0 ms. Planar gradient was then applied to improve the topographical representation of the SEF. It simplified the interpretation of the sensor-level data since the neuronal sources of the signals are typically situated directly below where the planar gradient is strongest (Wang et al., 2012). Additionally, this approach allows access to activations in a continuous set of sensors, which is necessary for subsequent cluster-based randomized permutation analysis. Briefly, the signals recorded from the axial gradiometer and the neighboring axial gradiometers (closer than 4 cm, typically six axial gradiometers) were used to get the planar gradient estimates for each sensor. Then, the root mean square was applied to combine the orthogonal components of the estimated planar gradient, obtaining positive values.

Stimulus intensity influences the topological representation of neural activity(McCarthy et al., 1985, Michel et al., 2004) (**Figure 8**). To study the evoked fields independent from stimulation intensity, the SEF was normalized using the root mean square (RMS normalization)(**Figure 9**). Briefly, for each participant, the root mean square (RMS) value was calculated across all channels at each time point. Subsequently, the data for each channel was divided by the RMS value to accomplish the normalization. Such that the effect of stimulus intensity is reduced, and brain activity evoked by electrical and pneumatic stimulation are more comparable.

$$\text{Normalized SEF}_{i,j}(t) = \frac{\text{SEF}_{i,j}(t)}{\sqrt{\frac{1}{N}\sum_{k=1}^{N} \text{SEF}_{k,j}(t)^2}}$$

$SEF_{i,j}(t)$ is the original SEF data for the i-th channel of the j-th participant at time point t. $\text{Normalized\_SEF}_{i,j}(t)$ is the normalized SEF data for the i-th channelof the j -th participant at time point t. N is the total number of

channels. $\sqrt{\frac{1}{N}\sum_{k=1}^{N} \mathrm{SEF}_{k,j}(t)^2}$ is the RMS value across all channels at time point t for the j-th participant, used to normalize the data for each channel.

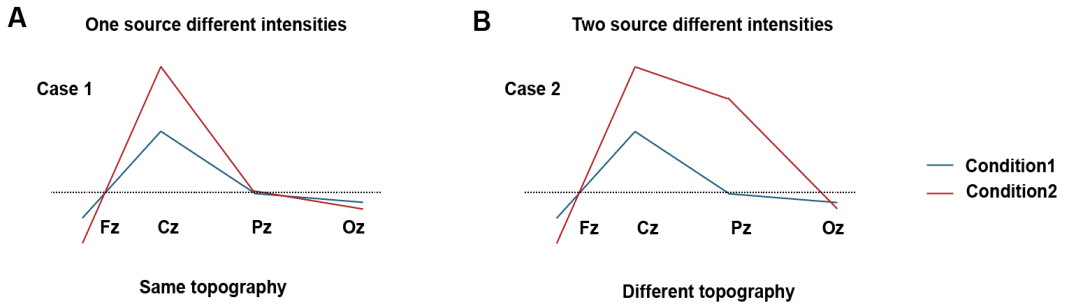

Figure 8. Effects of stimulus intensity on neural activity topographies with given source distributions. (A) one source with different stimulus intensities: the topography is the same, just linearly stretched. (B) two sources with different stimulus intensities: the topography is different.

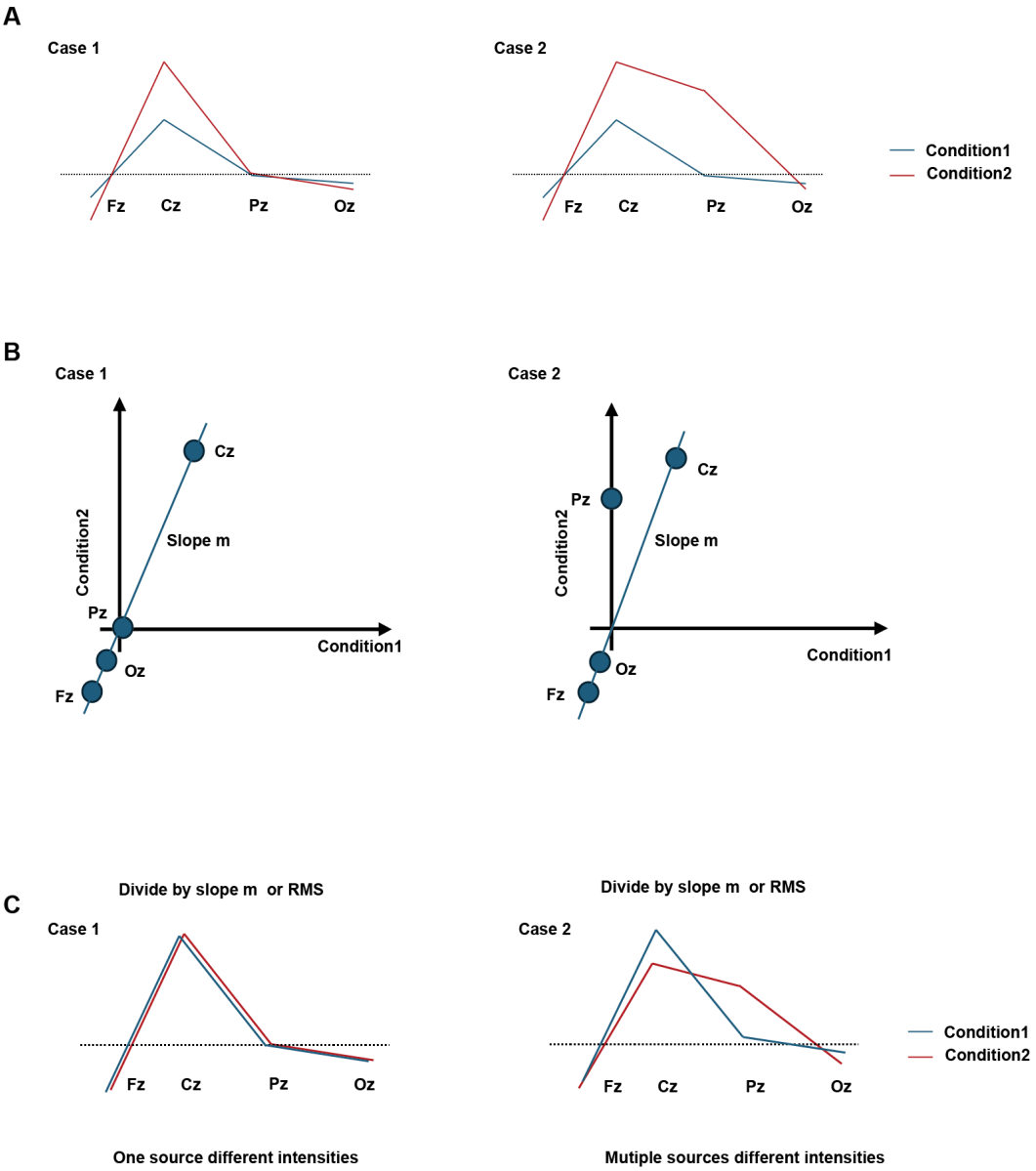

Figure 9. How to find out whether differences in topography are due to different intensities or different sources? (A) Effects of source distribution and stimulus intensity on neural activity topography. (B) Similarity analysis of neural activity between conditions was conducted to determine the slope **m**. (C) Normalization of neural activity was performed by dividing the data by either the slope **m** or the root mean square (RMS), thereby minimizing the influence of varying stimulus intensities on the topography. Following normalization, the results for Case 1 (left) indicate that the observed differences in topographies are attributed to variations in stimulus intensities. In contrast, the results for Case 2 (right) suggest that the differences in topographies arise from variations in source distribution.

2.6 Global mean field power (GMFP) and Signal to noise ratio (SNR)

To assess neural responses to pneumatic and electrical stimulation, the Global

Mean Field Power (GMFP) was computed for each participant across all channels. Subsequently, the Signal-to-Noise Ratio (SNR) was calculated based on the GMFP, which allows for the quantification of signal strength relative to baseline noise.

2.6.1. GMFP Calculation

The GMFP reflects the global field strength at each time point and is calculated as the spatial standard deviation of the event-related fields (ERF) across channels. The GMFP for a given participant at time point t is computed as follows:

$$GMFP(t, subj) = \sqrt{\frac{1}{N_{\text{channels}}} \sum_{ch=1}^{N_{\text{channels}}} \left(ERF(ch, t, subj) - \overline{ERF(t, subj)}\right)^2}$$

$GMFP\ (t,\ subj)$ is the GMFP at time point t for a given participant $subj$. $ERF\ (ch,\ t,\ subj)$ represents the ERF value at time point t for channel ch in the $subj$-th participant. $\overline{ERP(t, subj)}$ is the mean ERF value across all channels at time point t for the $subj$-th participant. $N_{channels}$ is the total number of channels.

2.6.2. SNR Calculation

The SNR for each participant was calculated using the GMFP within two time windows: the baseline period (-20ms to -10 ms) and the M20/M37 component period. The baseline GMFP represents the noise level, while the GMFP during the M20/M37 component represents the signal strength.

2.6.2.1 Signal Power

The signal power $\mathrm{P_{signal}(subj)}$ was calculated as the mean squared GMFP within the M20/M37 component time window. The formula for signal power is:

$$P_{\text{signal}}(subj) = \frac{1}{N_{\text{signal}}} \sum_{t=t_1}^{t_2} \left(GMFP(t, subj)\right)^2$$

t_1 and t_2 denote the start and end time points of the M20/M37 component. $\mathrm{N_{signal}}$ is the number of time points within the M20/M37 component.

2.6.2.2 Noise Power

Similarly, the noise power $\mathrm{P}_{noise}(\mathrm{subj})$ was computed as the mean squared GMFP during the baseline period (-20 ms to -10 ms):

$$P_{\text{noise}}(subj) = \frac{1}{N_{\text{baseline}}} \sum_{t=b_1}^{b_2} \left(GMFP(t, subj)\right)^2$$

b1 and b2 are the start and end time points of the baseline window (−20 ms to −10 ms). $\mathrm{N}_{\mathrm{baseline}}$ is the number of time points within the baseline window.

2.6.2.3 Signal-to-Noise Ratio (SNR)

The SNR for each participant was then computed as the ratio of the signal power to the noise power:

$$SNR(subj) = \frac{P_{\text{signal}}(subj)}{P_{\text{noise}}(subj)}$$

To express the SNR in decibels (dB), the following logarithmic transformation was applied:

$$SNR_{dB}(subj) = 10 \cdot \log_{10}\left(\frac{P_{\text{signal}}(subj)}{P_{\text{noise}}(subj)}\right)$$

2.7 Cluster-based permutation test

The cluster-based random permutation test was applied to compare differences in topographical descriptions between electrical and pneumatic stimuli at the sensor level. Based on the planar gradient estimation, the dependent t-test was used for each sensor, and all successive sensors that were smaller than the significance level (5%) were clustered. A null distribution that assumed no conditional differences was obtained by randomly permuting conditions among subjects 1024 times and computing the maximum cluster-level statistic for each permutation. Comparing the observed cluster-level statistics with the null distribution, significant clusters were identified as those at the highest or lowest 2.5th percentile. Here, positive clusters represent SEF amplitude at electrical stimulation higher than pneumatic stimulation, while negative clusters represent

SEF amplitude at electrical stimulation lower than pneumatic stimulation. This approach helped us to compare the activation differences at the sensor level between electrical and pneumatic stimulation within the time window of the M20 (median nerve) and M37 (tibial nerve) components.

2.8 Statistics

Spearman's rank correlation analysis quantified the consistency between the topographical distributions of SEFs for M20 (median nerve) and M37 (tibial nerve) under electrical and pneumatic stimulation. A normality test (Shapiro-Wilk) confirmed non-normal distribution of the data, justifying the use of a non-parametric method. Correlations were calculated between the topographical maps of M20 and M37 under each stimulation condition. A p-value below 0.05 was considered statistically significant. Topographic differences in SEFs between electrical and pneumatic stimulation of M20 (median nerve) and M37 (tibial nerve) were compared using a cluster-based random permutation test, with a two-tailed significance threshold of $p < 0.025$ (total $\alpha = 0.05$). Latency differences for M20 and M37 across conditions were evaluated using the Wilcoxon signed rank test, with $p < 0.05$ considered significant.

3 Results

3.1 Demographic characteristics of the participants

The demographic characteristics of the participants in this study are shown in **Table 1**. A total of 10 healthy adults were recruited for this study, 6 females and 4 males, with a mean age of (29.2 ± 2.0) years and a mean height of (167.5 ± 9.8) cm.

Participant (n=10)	Age (years)	Height (cm)	Arm span/2 (cm)	BMI (=kg/2)	Sex (F/M)
P1	29	171	87	25.0	M
P2	30	173	86	22.7	F
P3	25	170	84	22.1	M
P4	28	160	64	23.4	F
P5	30	167	82	21.5	F
P6	29	153	76.5	20.9	F
P7	31	172	87.5	20.3	F
P8	32	155	76	19.1	F
P9	31	187	93	26.3	M
P10	27	167	86.5	22.9	M
Average	**29.2 ± 2.0**	**167.5 ± 9.8**	**82.3 ± 8.2**	**22.4 ± 2.1**	**4 M+6F**

Table 1. A summary of participant characteristics.

3.2 Comparison of SEF axial topography under electrical and pneumatic stimulation of the median nerve

The axial plot of sensory evoked fields (SEF) for median nerve stimulation was analyzed under electrical and pneumatic conditions. In these plots, the M20 component waveform under electrical stimulation **(Figure 10A)**. was clear and sharp, while the waveform under pneumatic stimulation was less distinct **(Figure 10B)**. The signal-to-noise ratio (SNR) of the M20 component in axial gradient under electrical stimulation (14.8492 dB) is significantly higher (p-value = 0.00056) than that under pneumatic stimulation (9.0187 dB).(**Figure 10C**).

Next, we used cluster analysis to compare the differences in the M20 component on the axial topography. Without normalizing stimulus intensity, the cluster analysis revealed a statistically significant difference in amplitude for the M20 component between electrical and pneumatic stimulation conditions. Specifically, the amplitude of M20 under electrical stimulation was higher than under pneumatic stimulation **(P<0.025, Figure 11A)**. However, after normalizing stimulus intensity, no significant difference in M20 was observed between the two stimulation conditions **(P>0.025, Figure 11B)**.

Finally, we conducted a Spearman's analysis to assess the correlation of M20 axial topography between electrical and pneumatic stimulation conditions. The results demonstrated a high correlation between the M20 components in both non-normalized and normalized conditions. Additionally, the correlation in the non-normalized condition was higher than in the normalized condition **(P<0.01, Figures 12 and 13).**

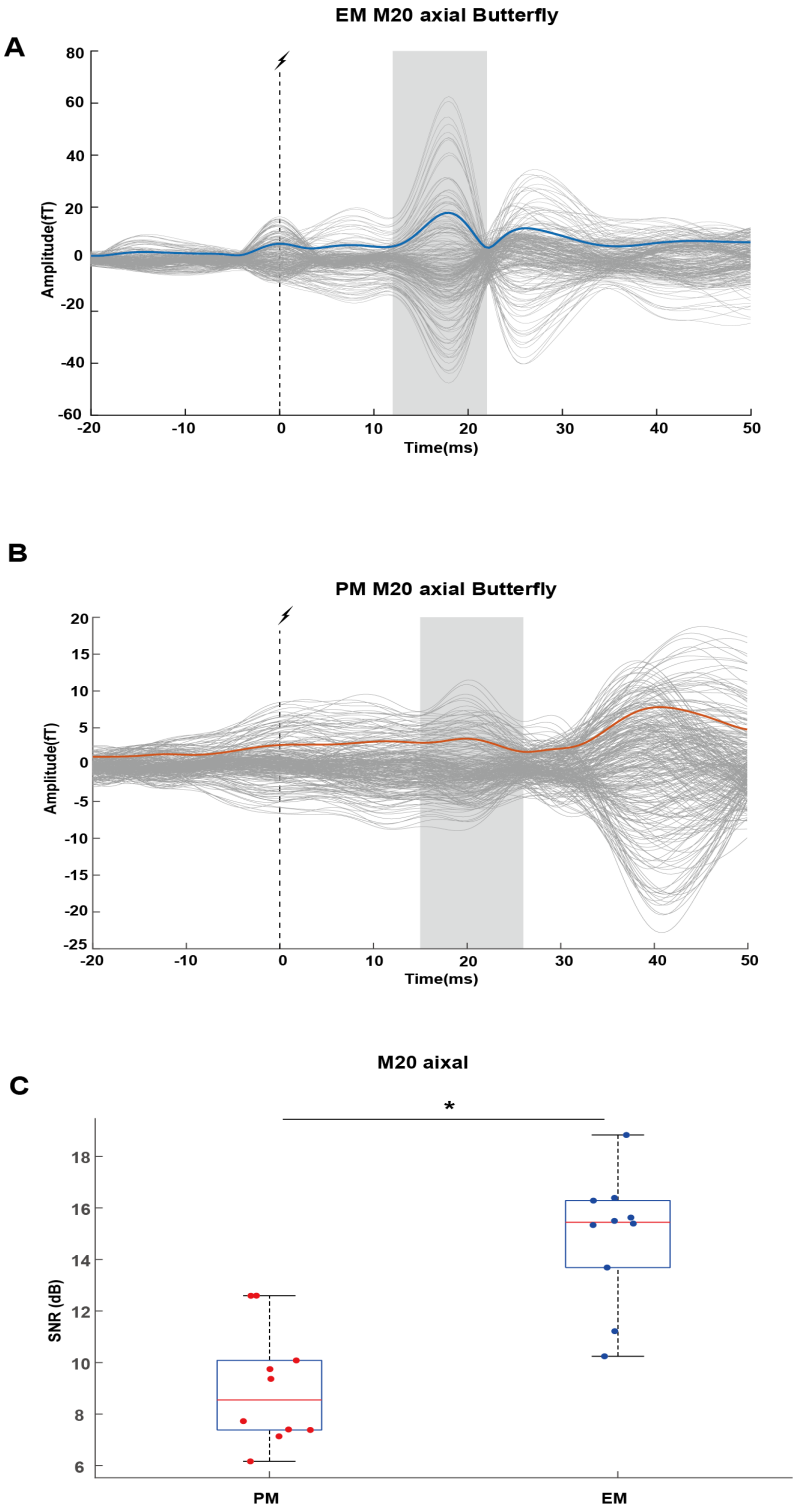

Figure 10. Axial butterfly plots of SEF under electrical stimulation (EM) and pneumatic stimulation (PM) of the median nerve; (A) Axial SEF butterfly plot and global mean field power (GMFP) for EM (blue curve); (B) Axial SEF butterfly plot and GMFP for PM (red curve); Gray bars represent the M20 component of the SEF. The dotted line in (A) and (B) indicates the stimulation onset. (C) The signal-to-noise ratio (SNR) of the M20 component in axial gradient under electrical (EM) and pneumatic stimulation (PM) of the median nerve.

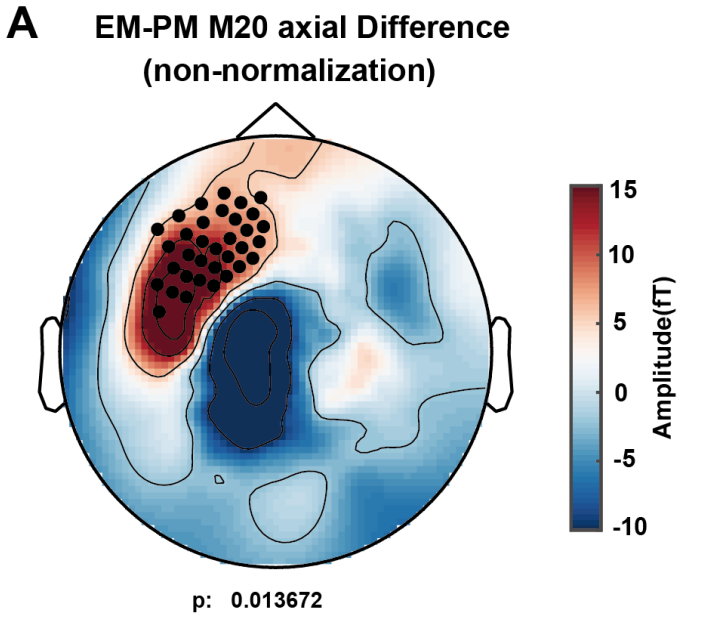

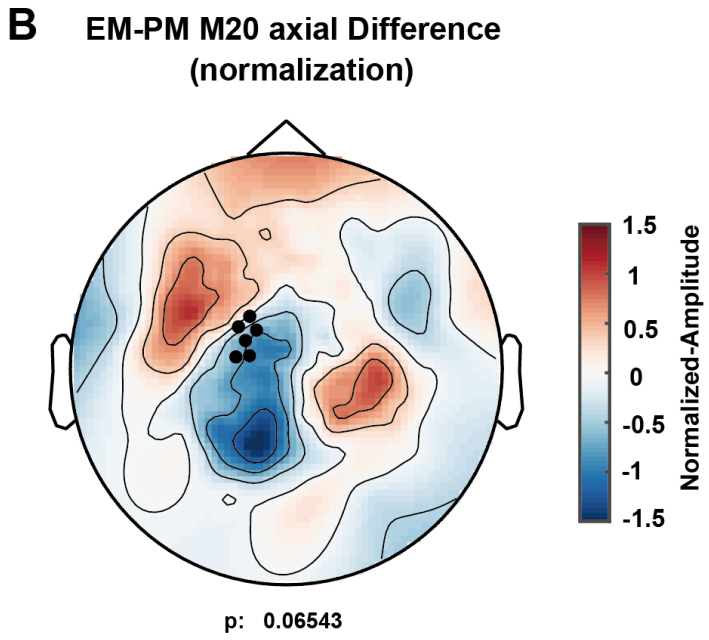

Figure 11. Cluster analysis of M20 component on axial topography; (A) Amplitude differences of M20 topography under electrical stimulation (EM) and pneumatic stimulation (PM) of the median nerve, without normalizing stimulus intensity; (B) Amplitude differences of M20 topography under electrical stimulation (EM) and pneumatic stimulation (PM) of the median nerve, after normalizing stimulus intensity; The color bar displays the range of amplitudes corresponding to the colors. Black dots indicate sensors with significant higher amplitude of the M20 component in axial gradient under electrical stimulation compared to pneumatic stimulation.

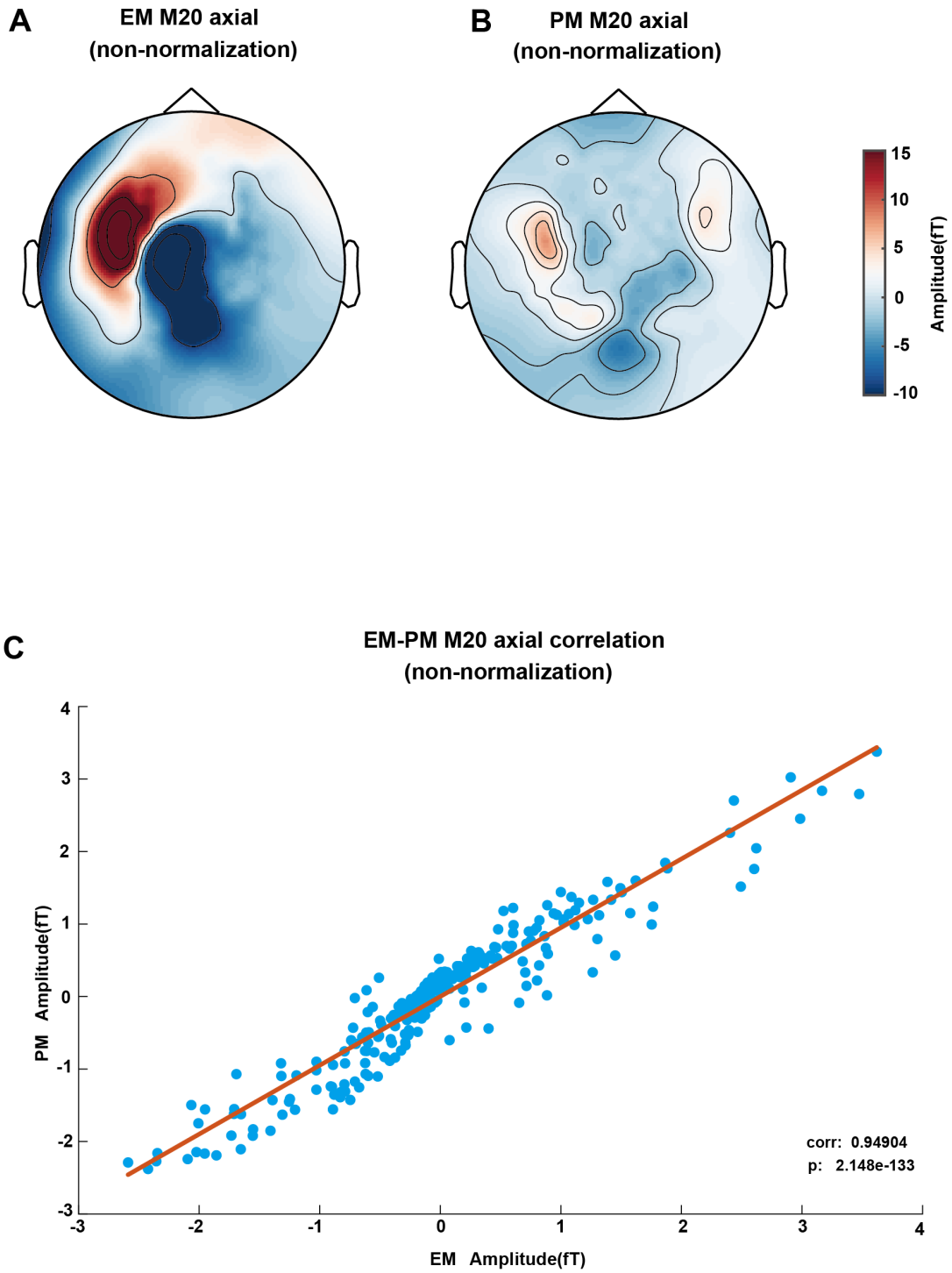

Figure 12. Correlation analysis of M20 axial topography under electrical and pneumatic stimulation with non-normalized stimulus intensity; (A) Axial topography of M20 under electrical stimulation, non-normalized stimulus intensity; (B) Axial topography of M20 under pneumatic stimulation, non-normalized stimulus intensity; (C) Statistical correlation in axial topography of M20 under electrical and pneumatic stimulation with non-normalized stimulus intensities.

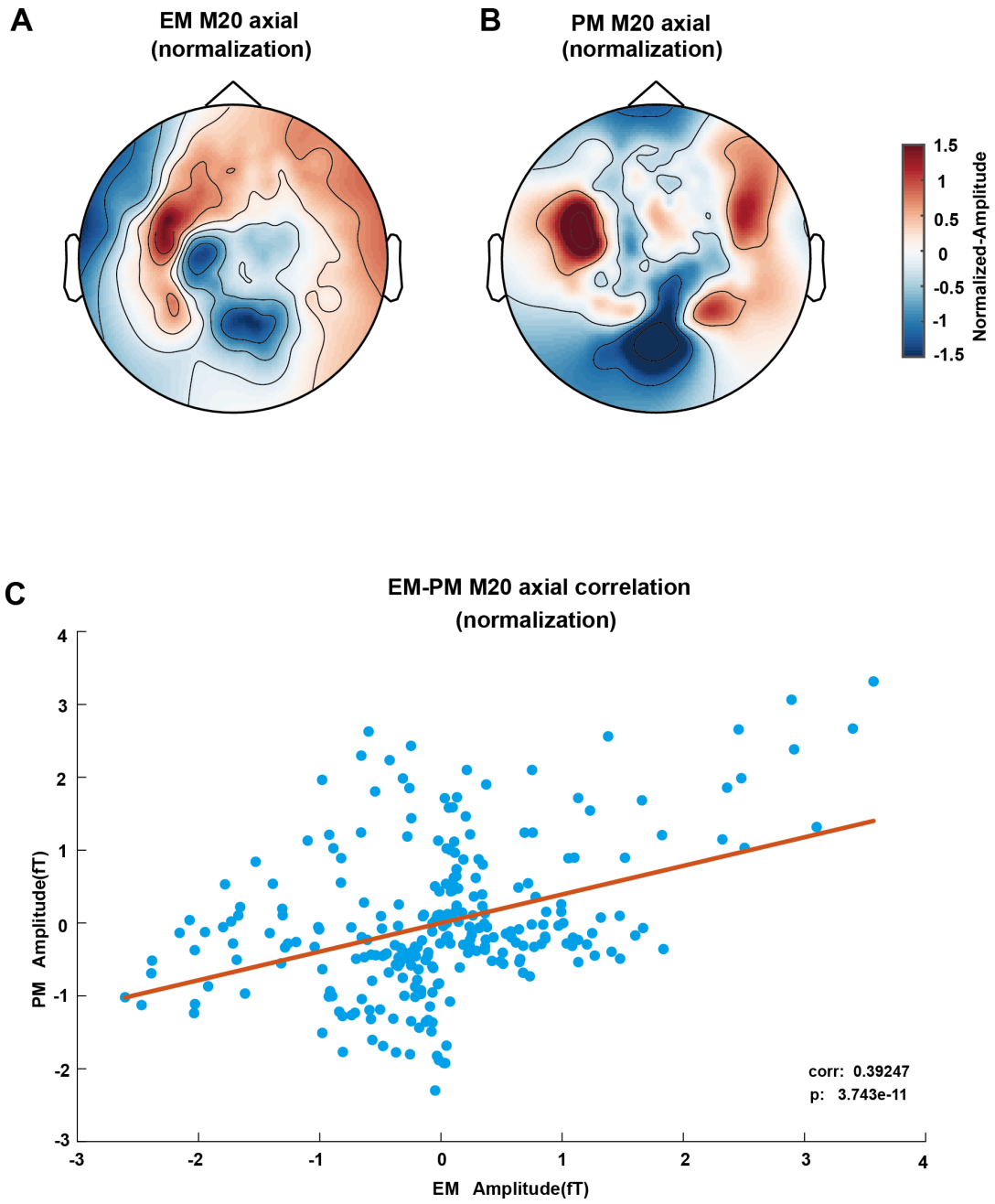

Figure 13. Correlation analysis of M20 axial topography under electrical and pneumatic stimulation with normalized stimulus intensity; (A) Axial topography of M20 under electrical stimulation, normalized stimulus intensity; (B) Axial topography of M20 under pneumatic stimulation, normalized stimulus intensity; (C) Statistical correlation in axial topography of M20 under electrical and pneumatic stimulation with normalized stimulus intensities.

3.3 Comparison of SEF planar topography under electrical and pneumatic stimulation of the median nerve

The planar plot of sensory evoked fields (SEF) for median nerve stimulation was analyzed under electrical and pneumatic conditions.The SEF's butterfly plot under electrical stimulation **(Figure 14A)** showed a clear and distinct waveform of the M20 component, whereas, under pneumatic stimulation **(Figure 14B)**, the M20 component appeared flat or blurry**.** The signal-to-noise ratio (SNR) of the M20 component in planar gradient under electrical stimulation (15.4666 dB) is significantly higher (p-value = 0.0016675) than that under pneumatic stimulation (9.4714 dB).(**Figure 14C**).

Cluster analysis demonstrated a statistically significant difference in M20 planar topography between electrical and pneumatic stimulation conditions before normalizing stimulus intensity. Specifically, the amplitude of M20 was higher under electrical stimulation than pneumatic stimulation **(P<0.025, Figure 15A).** However, no statistical difference was found between the two conditions after normalizing stimulus intensity **(P>0.025, Figure 15B).**

Correlation analyses revealed a high correlation between the M20 components under electrical and pneumatic stimulation conditions, both at non-normalized and normalized stimulus intensities. Furthermore, the correlation at non-normalized stimulus intensity was higher than at normalized intensity. These findings are consistent with our axial map analyses **(P<0.01, Figures 16 and 17).**

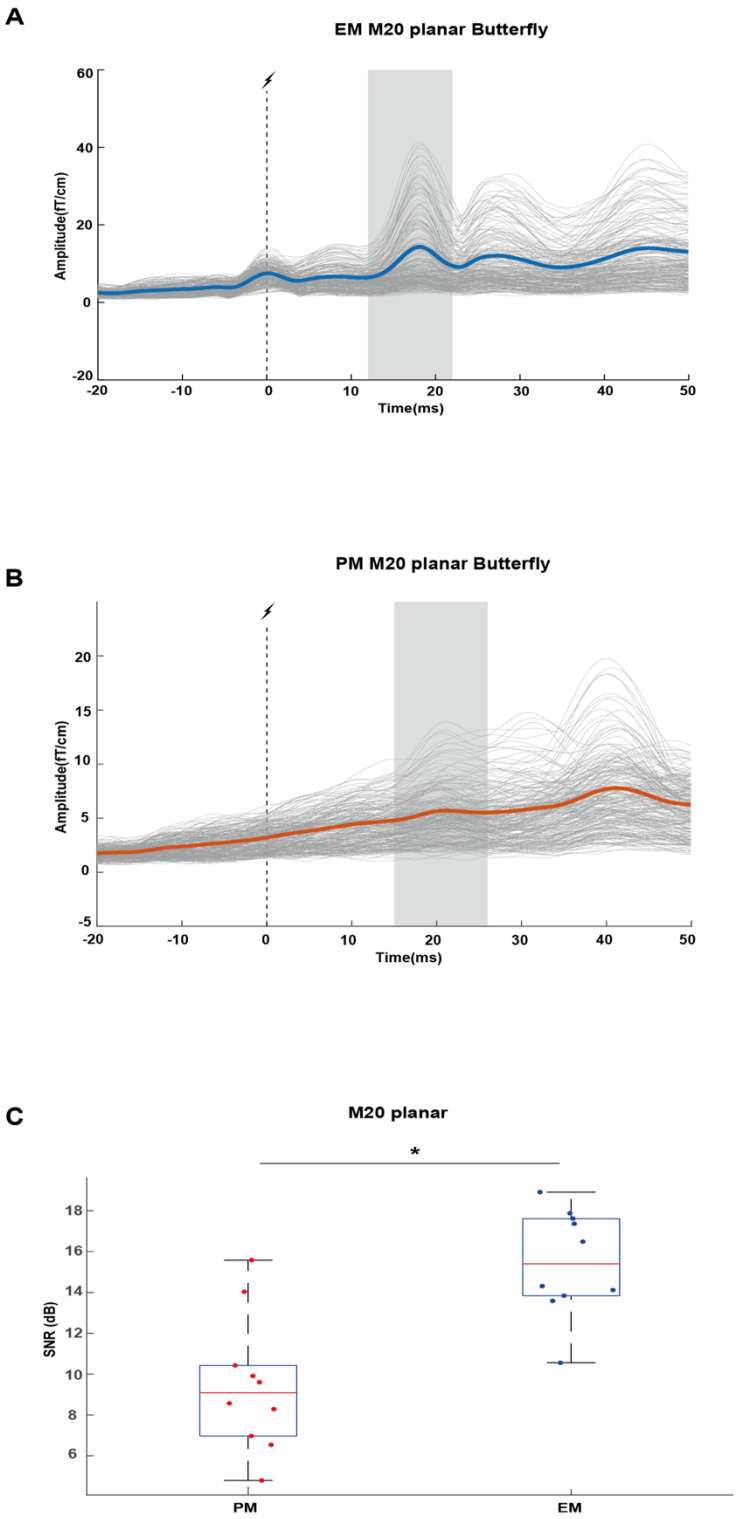

Figure 14. Planar butterfly plots of SEF under electrical stimulation (EM) and pneumatic stimulation (PM) of the median nerve; (A) Planar SEF butterfly plot and global mean field power (GMFP) for EM (blue curve); (B) Planar SEF butterfly plot and GMFP for PM (red curve). Gray bars represent the M20 component of the SEF. The dotted line in (A) and (B) indicates the stimulation onset. (C) The signal-to-noise ratio (SNR) of the M20 component in planar gradient under electrical (EM) and pneumatic stimulation (PM) of the median nerve.

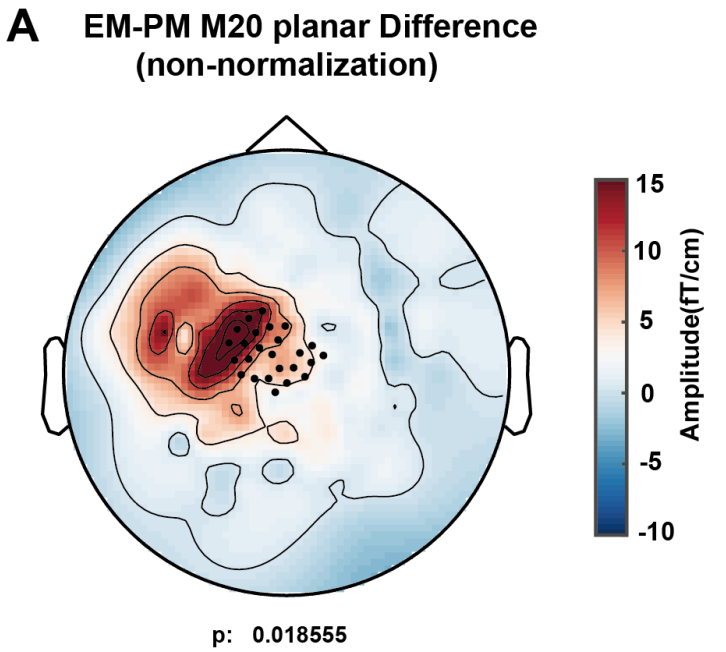

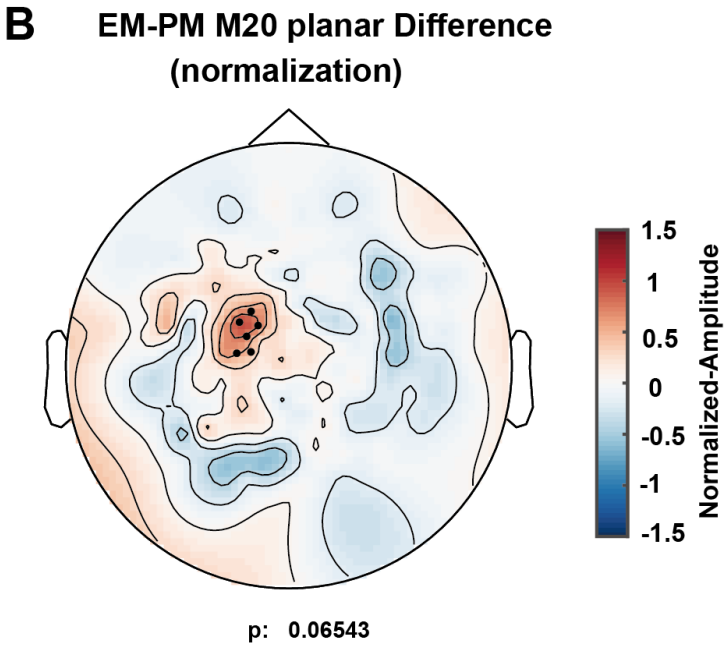

Figure 15. Cluster analysis of M20 component on planar topography; (A) Amplitude differences of M20 planar under electrical stimulation and pneumatic stimulation without normalizing stimulus intensity; (B) Amplitude differences of M20 topography under electrical stimulation (EM) and pneumatic stimulation (PM), after normalizing stimulus intensity. The color bar displays the range of amplitudes corresponding to the colors. Black dots indicate sensors with significant higher amplitude of the M20 component in planar gradient under electrical stimulation compared to pneumatic stimulation.

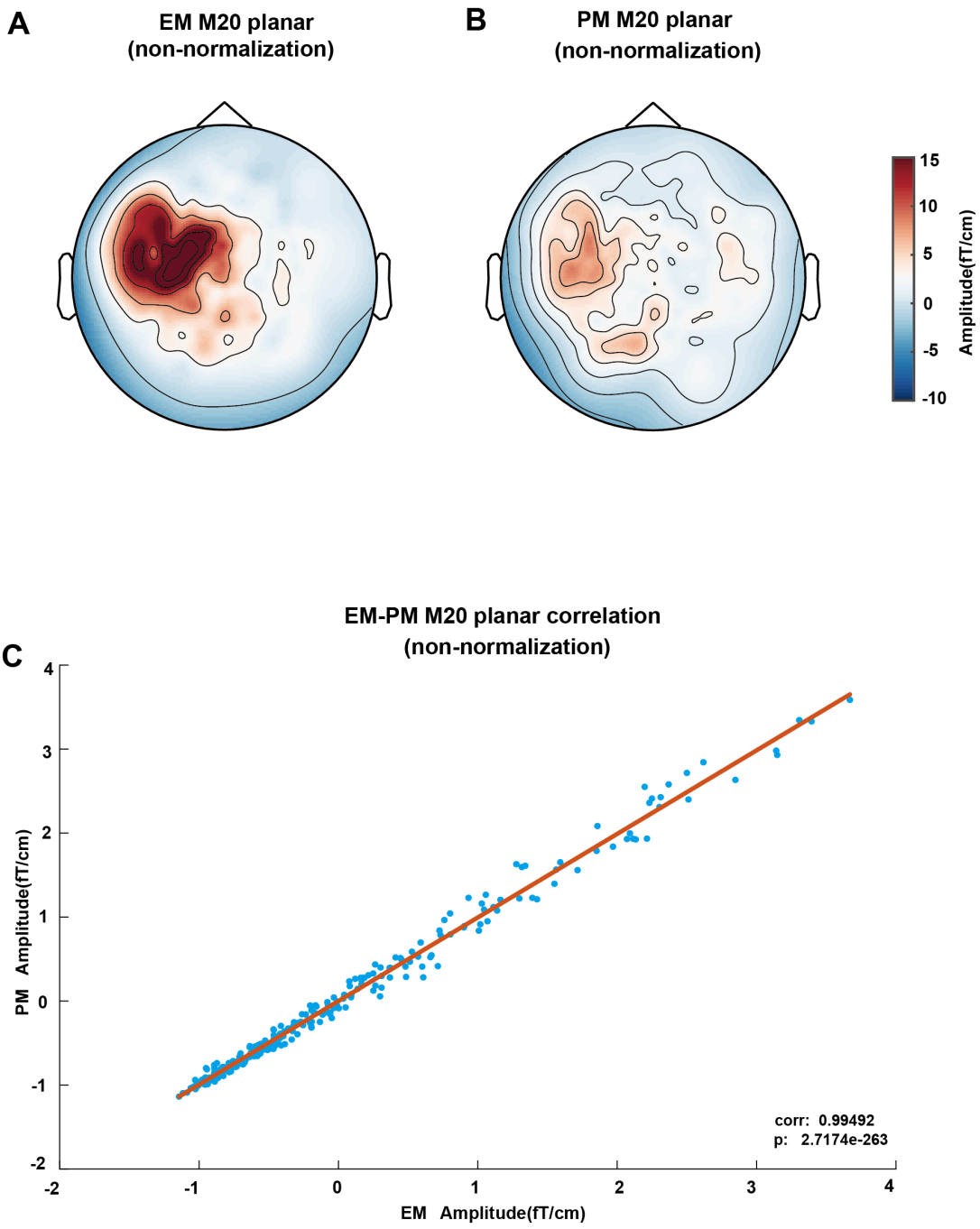

Figure 16. Correlation analysis of M20 planar topography under electrical and pneumatic stimulation without normalized stimulus intensity; (A) planar topography of M20 under electrical stimulation, non-normalized stimulus intensity; (B) planar topography of M20 under pneumatic stimulation, non-normalized stimulus intensity; (C) Statistical correlation of M20 planar topography under electrical and pneumatic stimulation with non-normalized stimulus intensities.

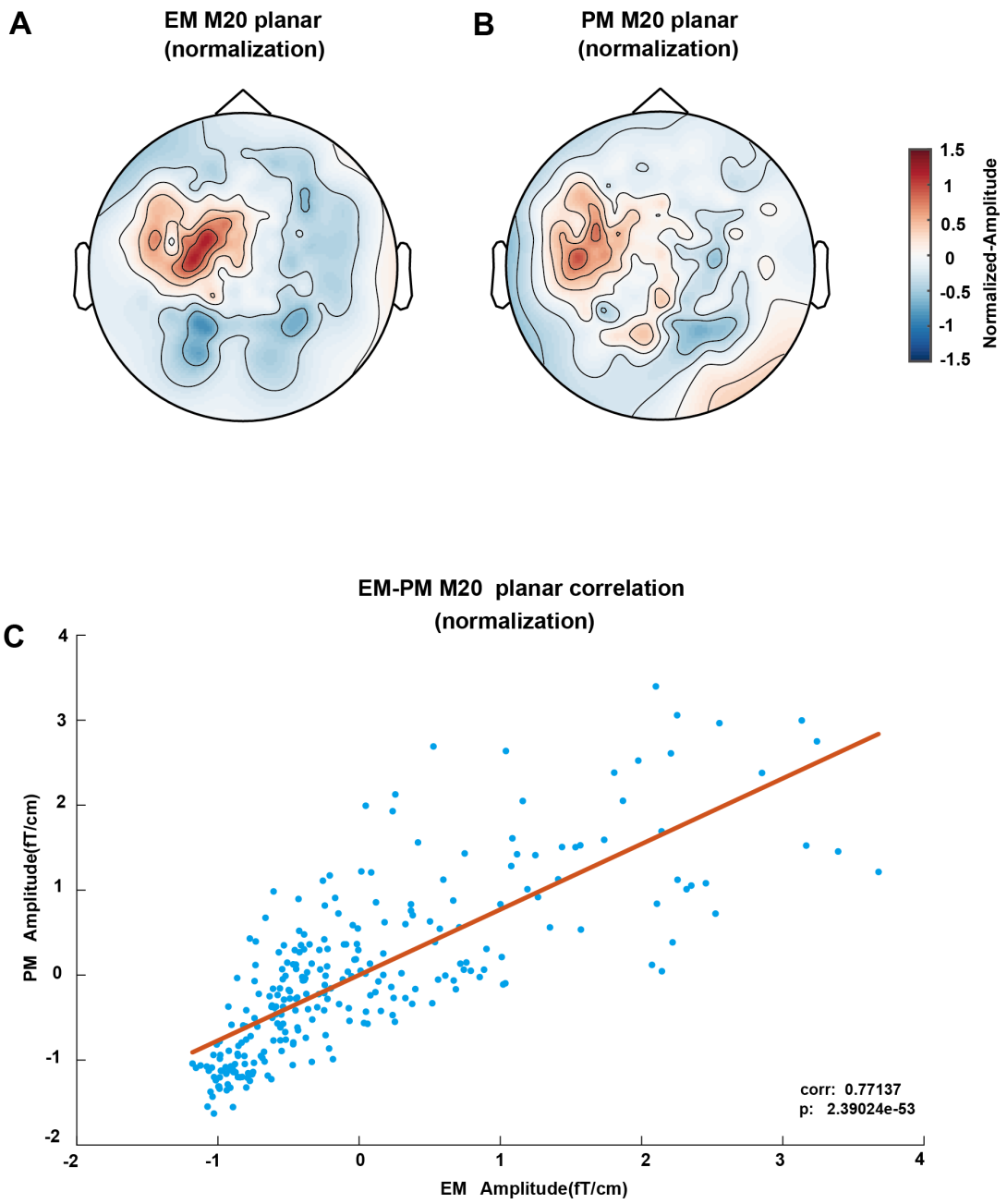

Figure 17. Correlation analysis of M20 planar topography under electrical and pneumatic stimulation with normalized stimulus intensity; (A) planar topography of M20 under electrical stimulation, normalized stimulus intensity; (B) planar topography of M20 under pneumatic stimulation, normalized stimulus intensity; (C) Statistical correlation in planar topography of M20 under electrical and pneumatic stimulation with normalized stimulus intensities.

3.4 Comparison of SEF axial topography under electrical and pneumatic stimulation of the tibial nerve

The axial plot of sensory evoked fields (SEF) for tibial nerve stimulation was analyzed under electrical and pneumatic conditions. Under electrical stimulation **(Figure 18A)**, the SEF axial plot displayed a clear and well-defined waveform for the M37 component, whereas, under pneumatic stimulation **(Figure 18B)**, the M37 waveform was very flat**.** The signal-to-noise ratio (SNR) of the M37 component in axial gradient under electrical stimulation (9.9095 dB) is significantly higher (p-value = 0.011349) than that under pneumatic stimulation (7.3389 dB).(**Figure 18C**).

Cluster analysis revealed no statistical difference in the M37 component between electrical and pneumatic stimulation conditions, whether the stimulus intensities were non-normalized or normalized **(P>0.025, Figure 17).**

Correlation analysis of the axial plots revealed a high correlation between M37 under electrical stimulation and M37 under pneumatic stimulation when stimulus intensities were not normalized **(P<0.01, Figure 20)**. However, after normalizing the stimulus intensity, no correlation was found between M37 under the two conditions **(P>0.05, Figure 21).**

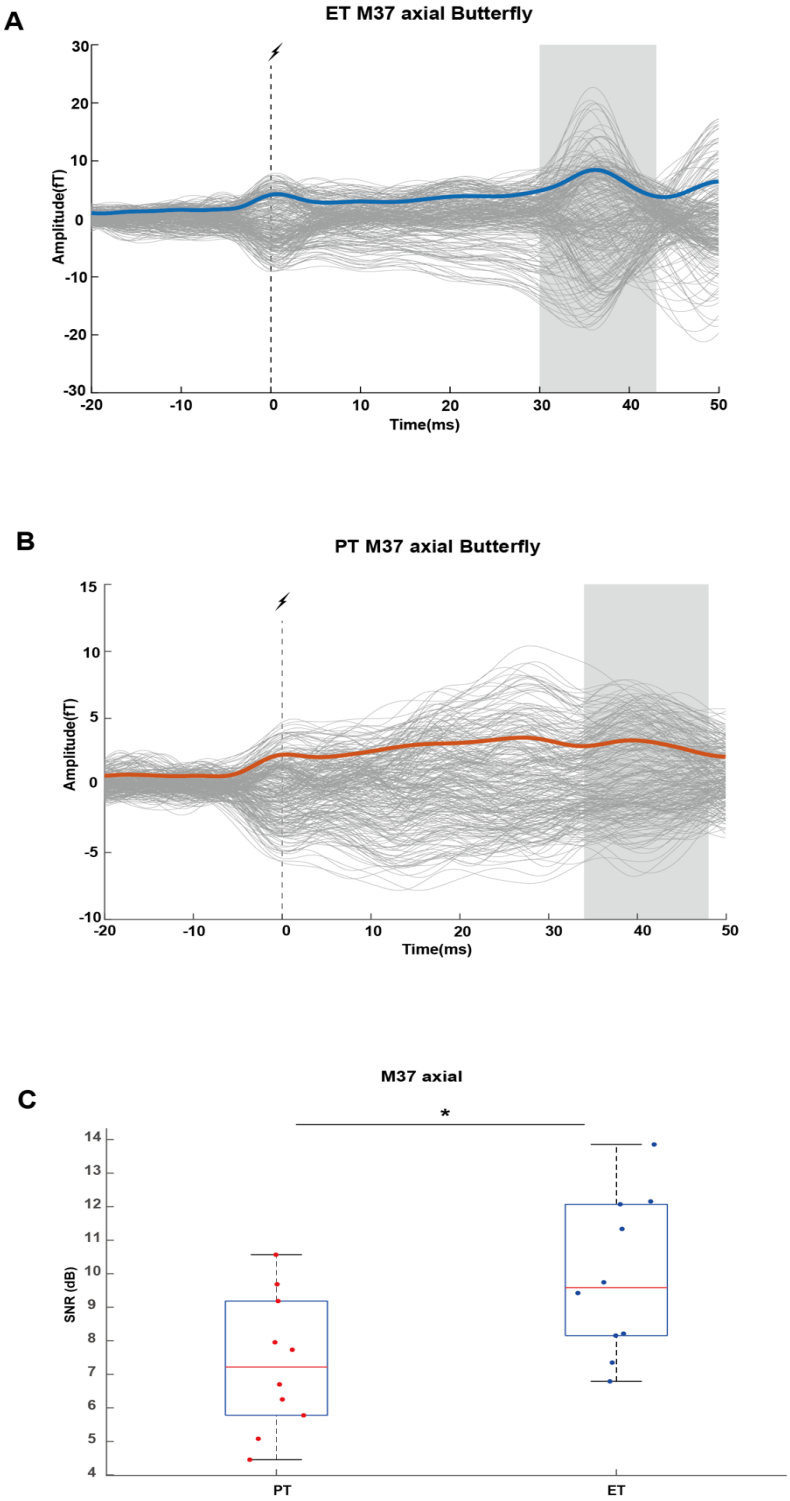

Figure 18. Axial butterfly plots of SEF under electrical stimulation (ET) and pneumatic stimulation (PT) of the tibial nerve; (A) Axial SEF butterfly plot and global mean field power (GMFP) for ET (blue curve); (B) Axial SEF butterfly plot and GMFP for PM (red curve). Gray bars represent the SEF component M37. The dotted line in (A) and (B) indicates the stimulation onset. (C) The signal-to-noise ratio (SNR) of the M37 component in axial gradient under electrical (ET) and pneumatic stimulation (PT) of the tibial nerve.

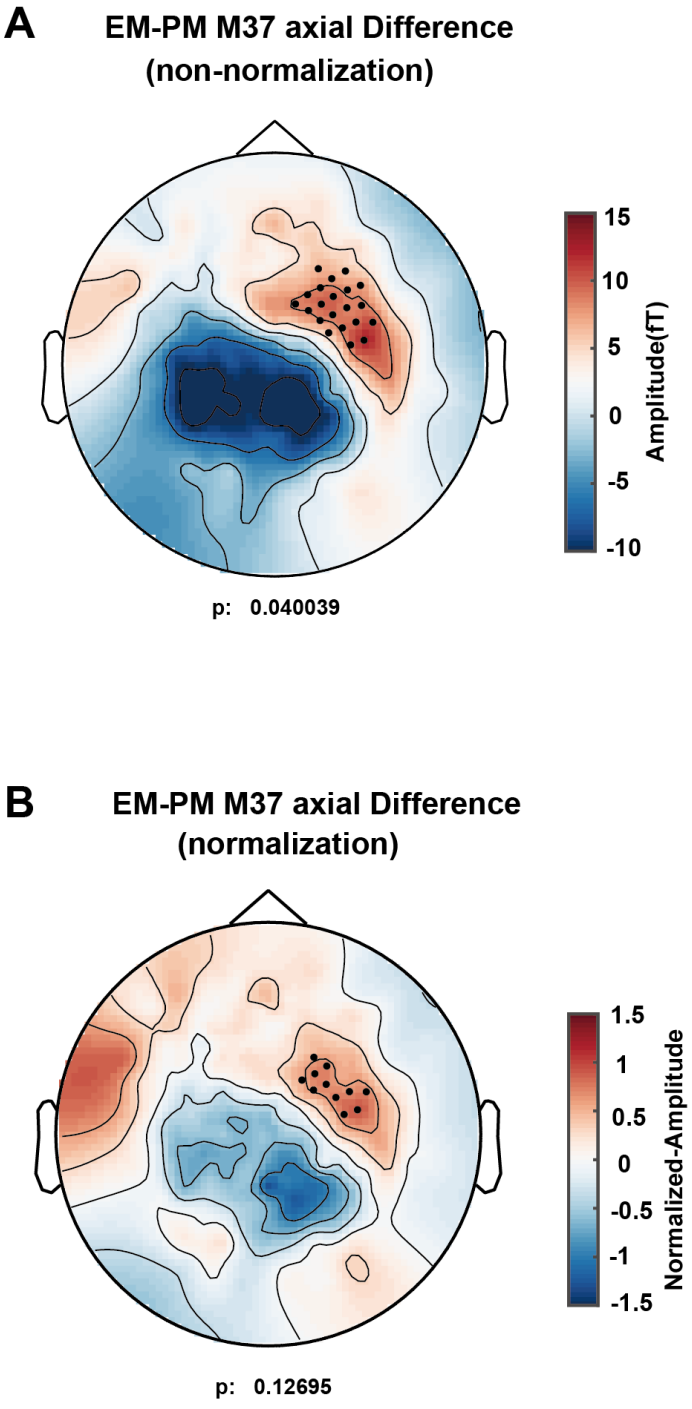

Figure 19. Cluster analysis of M37 component on axial topography; (A) Amplitude differences of M37 topography under electrical and pneumatic stimulation, without normalizing stimulus intensity; (B) Amplitude differences of M37 topography under electrical and pneumatic stimulation after normalizing stimulus intensity; The color bar displays the range of amplitudes corresponding to the colors. Black dots indicate sensors with significant higher amplitude of the M37 component in axial gradient under electrical stimulation compared to pneumatic stimulation.

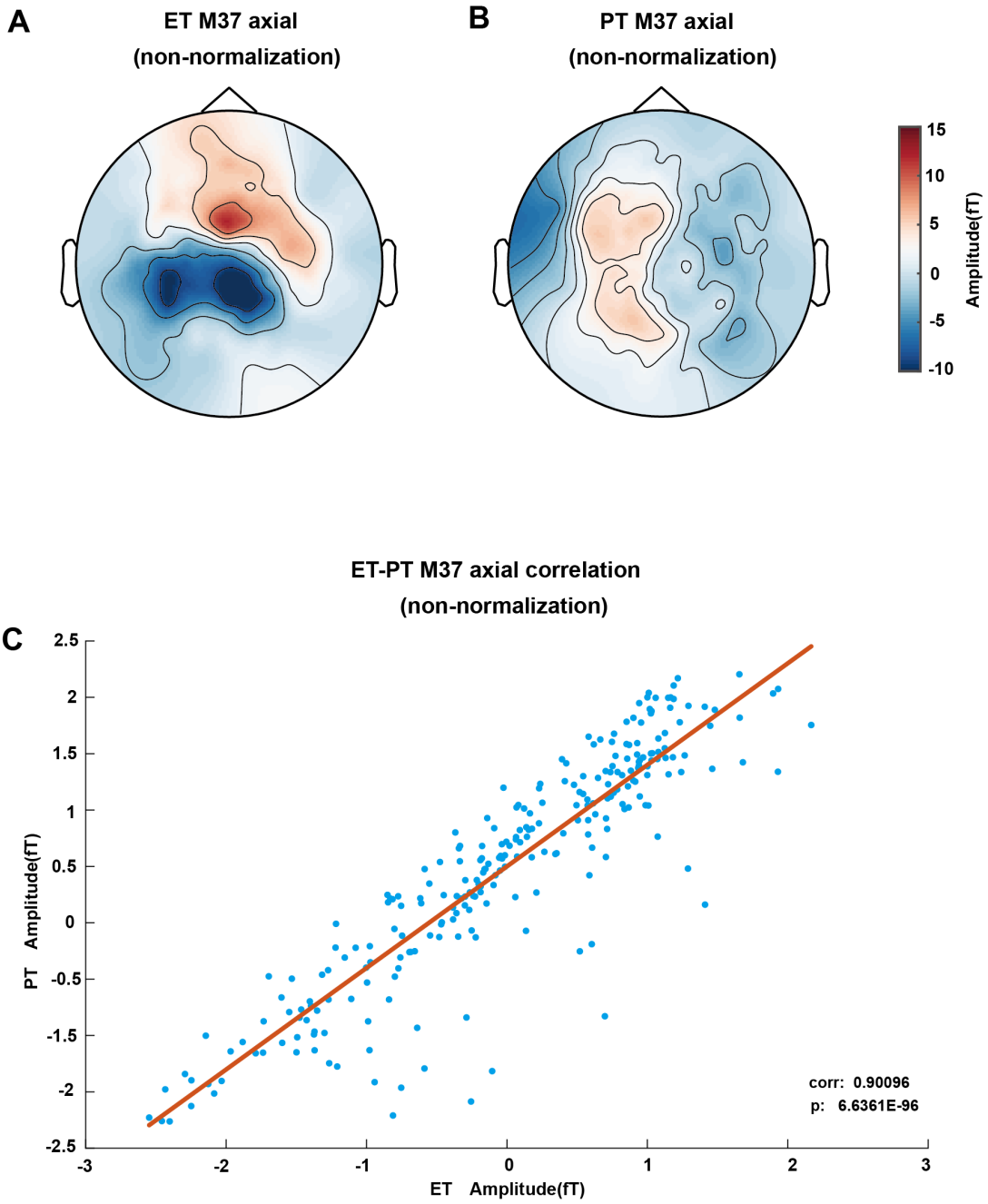

Figure 20. Correlation analysis of M37 axial topography under electrical and pneumatic stimulation with non-normalized stimulus intensity; (A) Axial topography of M37 under electrical stimulation, non-normalized stimulus intensity; (B) Axial topography of M37 under pneumatic stimulation, non-normalized stimulus intensity; (C) Statistical correlation in axial topography of M37 under electrical and pneumatic stimulation with non-normalized stimulus intensities.

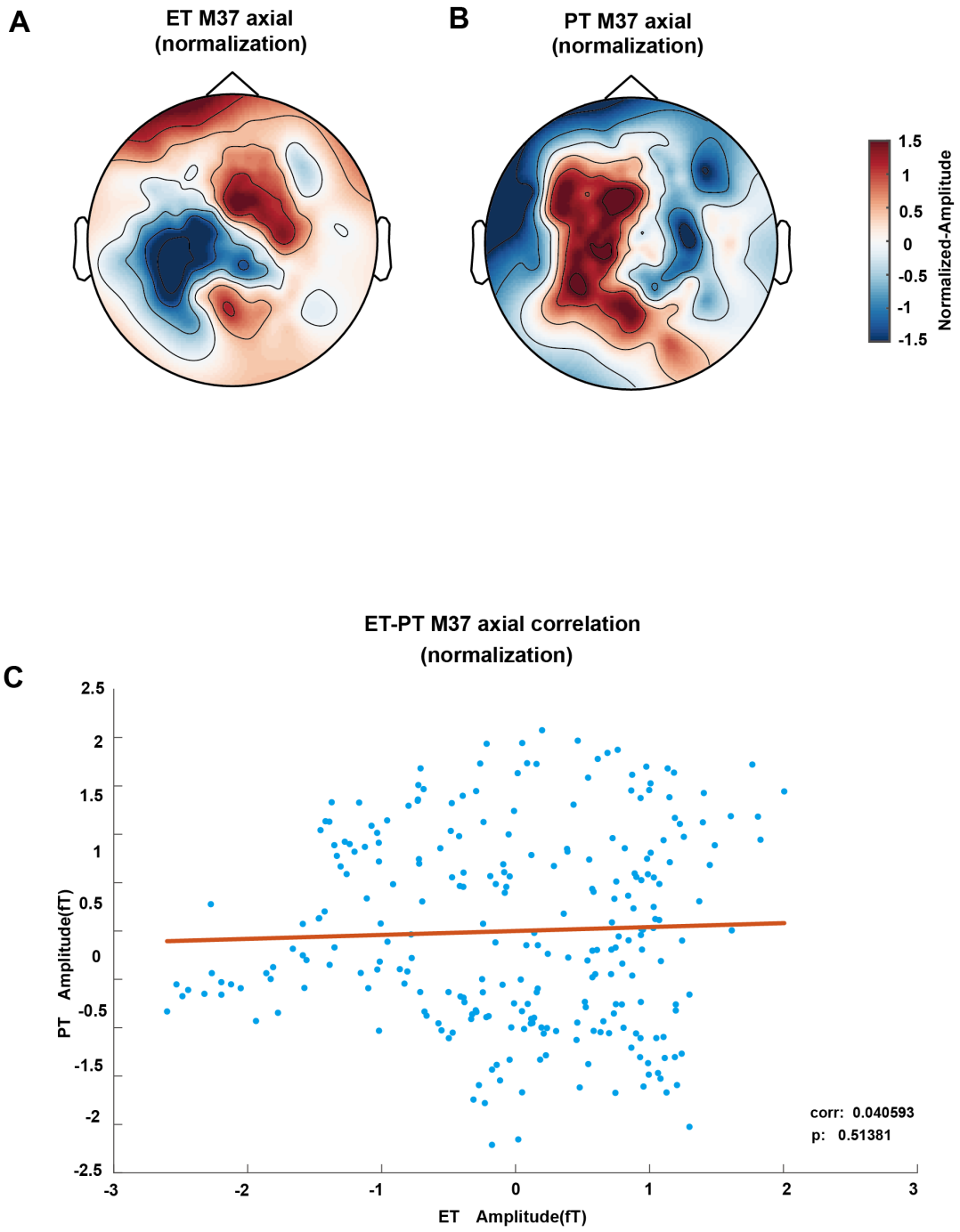

Figure 21. Correlation analysis of M37 axial topography under electrical and pneumatic stimulation with normalized stimulus intensity; (A) Axial topography of M37 under electrical stimulation after normalized stimulus intensity; (B) Axial topography of M37 under pneumatic stimulation after normalized stimulus intensity; (C) No statistical correlation in axial topography of M37 component under electrical and pneumatic stimulation with normalized stimulus intensities.

3.5 Comparison of SEF planar topography under electrical and pneumatic stimulation of the tibial nerve

The planar plot of sensory evoked fields (SEF) for tibial nerve stimulation was analyzed under electrical and pneumatic conditions.The SEF planar plots showed a clearer and more defined waveform of the M37 component in the electrical stimulation **(Figure 22A)**condition compared to pneumatic stimulation **(Figure 22B).** The signal-to-noise ratio (SNR) of the M37 component in planar gradient under electrical stimulation (10.0479 dB) is significantly higher (p-value = 0.018958) than that under pneumatic stimulation (7.5072 dB).(**Figure 22C**).

Cluster analysis indicated statistically significant differences in the topography of the M37 component between electrical and pneumatic stimulation conditions when stimulus intensity was not normalized. Specifically, the amplitude of SEF component M37 was higher under electrical stimulation than under pneumatic stimulation **(P<0.025, Figure 23A).** After normalizing stimulus intensity, however, the planar plots of the M37 component between electrical and pneumatic stimulation conditions did not show a statistically significant difference **(P>0.025, Figure 23B).**

Correlation analyses of the planar maps indicated that M37 under electrical and pneumatic stimulation conditions exhibited significant correlation at both un-normalized and normalized stimulus intensities. Moreover, the correlation at normalized stimulus intensity was higher than for non-normalized ones **(P<0.01, Figures 24 and 25).**

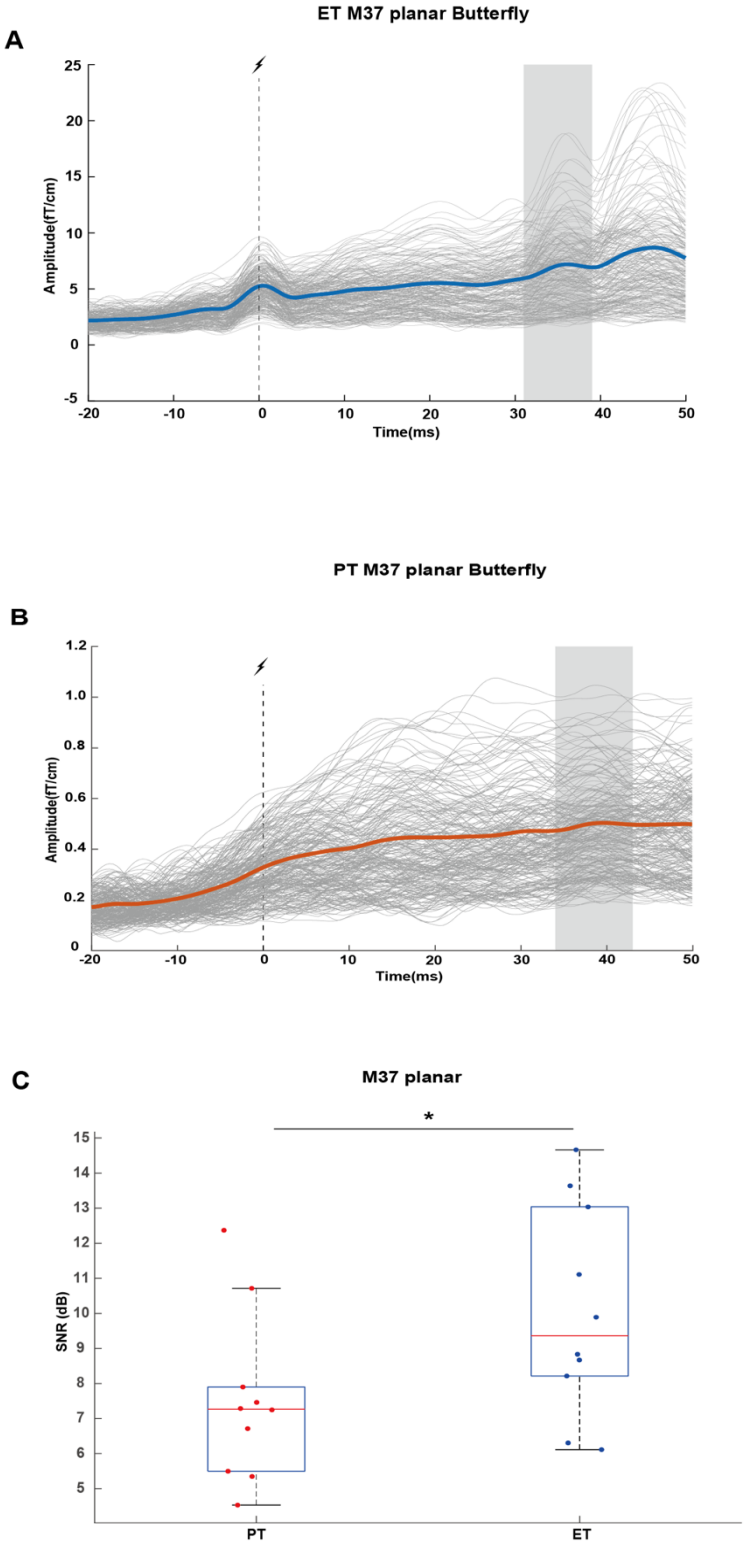

Figure 22. Planar butterfly plots of SEF under electrical stimulation (ET) and pneumatic stimulation (PT) of the tibial nerve; (A) Planar SEF butterfly plot and global mean field power (GMFP) for ET (blue curve); (B) Planar SEF butterfly plot and GMFP for PT (red curve). Gray bars represent the M37 component of the SEF. The dotted line in (A) and (B) indicates the stimulation onset. (C) The signal-to-noise ratio (SNR) of the M37 component in planar gradient under electrical (ET) and pneumatic stimulation (PT) of the tibial nerve.

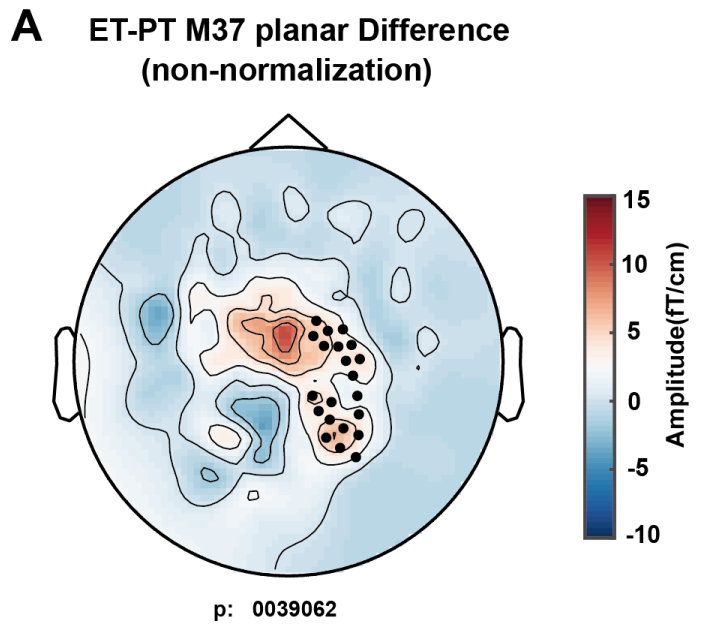

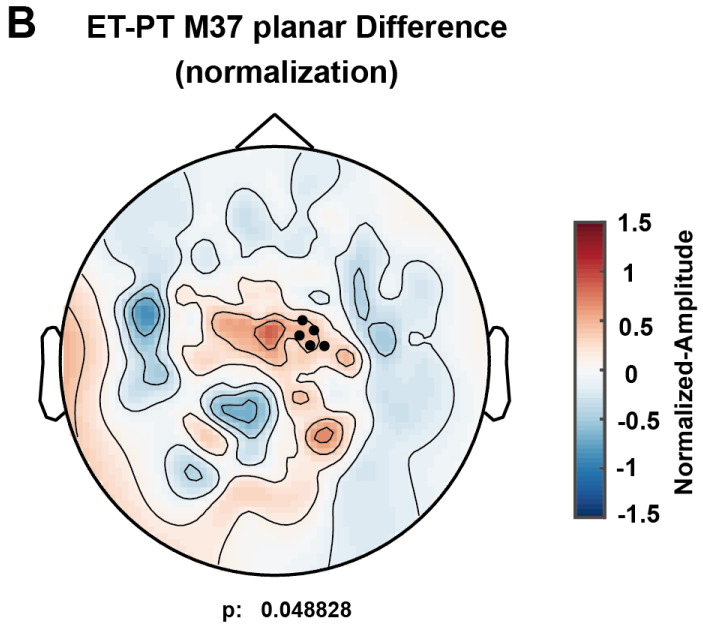

Figure 23. Cluster analysis of M37 component on planar topography; (A) Amplitude differences of M37 planar under electrical stimulation and pneumatic stimulation without normalizing stimulus intensity; (B) Amplitude differences of M37 topography under electrical stimulation (EM) and pneumatic stimulation (PM), after normalizing stimulus intensity; Black dots indicate sensors with significant amplitude differences between the two types of stimulation.

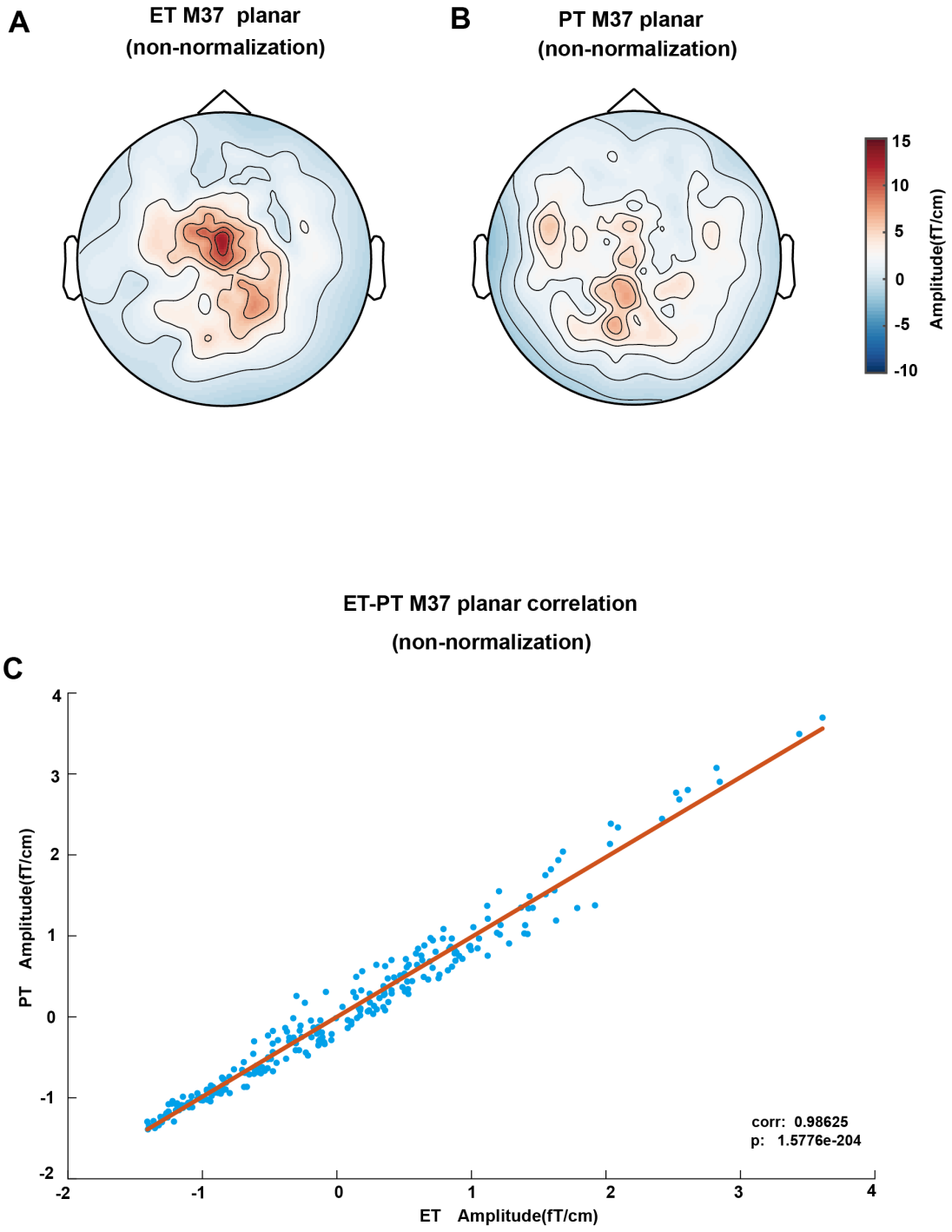

Figure 24. Correlation analysis of M37 planar topography under electrical and pneumatic stimulation without normalized stimulus intensity; (A) planar topography of M37 under electrical stimulation, non-normalized stimulus intensity; (B) planar topography of M37 under pneumatic stimulation, non-normalized stimulus intensity; (C) Statistical correlation of M37 planar topography under electrical and pneumatic stimulation with non-normalized stimulus intensities.

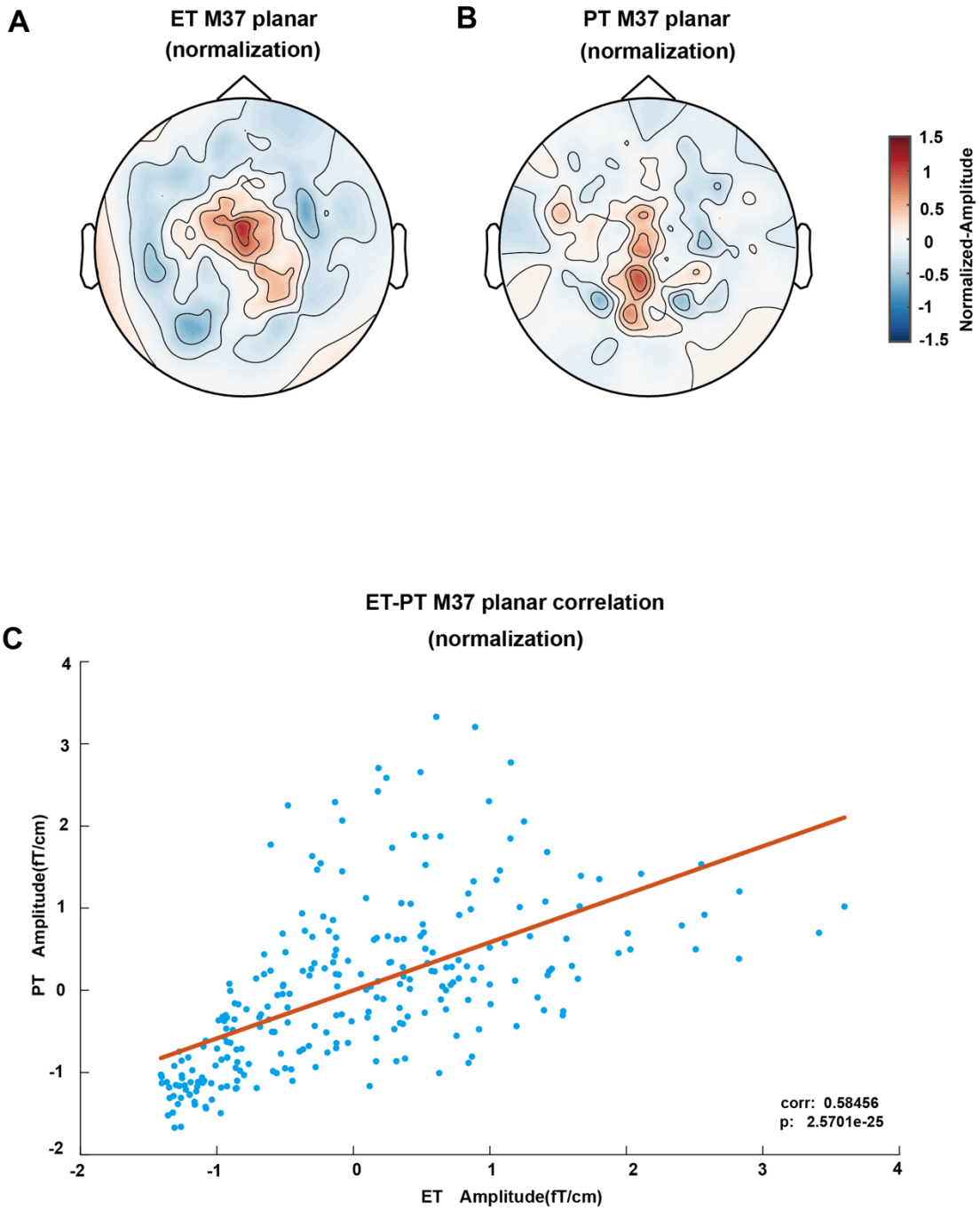

Figure 25. Correlation analysis of M37 planar topography under electrical and pneumatic stimulation with normalized stimulus intensity; (A) planar topography of M37 under electrical stimulation, normalized stimulus intensity; (B) planar topography of M37 under pneumatic stimulation, normalized stimulus intensity; (C) Statistical correlation in planar topography of M37 under electrical and pneumatic stimulation with normalized stimulus intensities.

3.6 Comparison of M20 and M37 latency under electrical and pneumatic stimulation

In both the axial and planar topographies, the latencies of the M20 component under pneumatic stimulation were significantly longer than under electrical stimulation **(P<0.05, Figure 26A and 26B)**. Similarly, for the M37 component, the latencies under pneumatic stimulation were significantly longer than under electrical stimulation in both axial and planar topographies **(P<0.05, Figure 26C and 26D).**

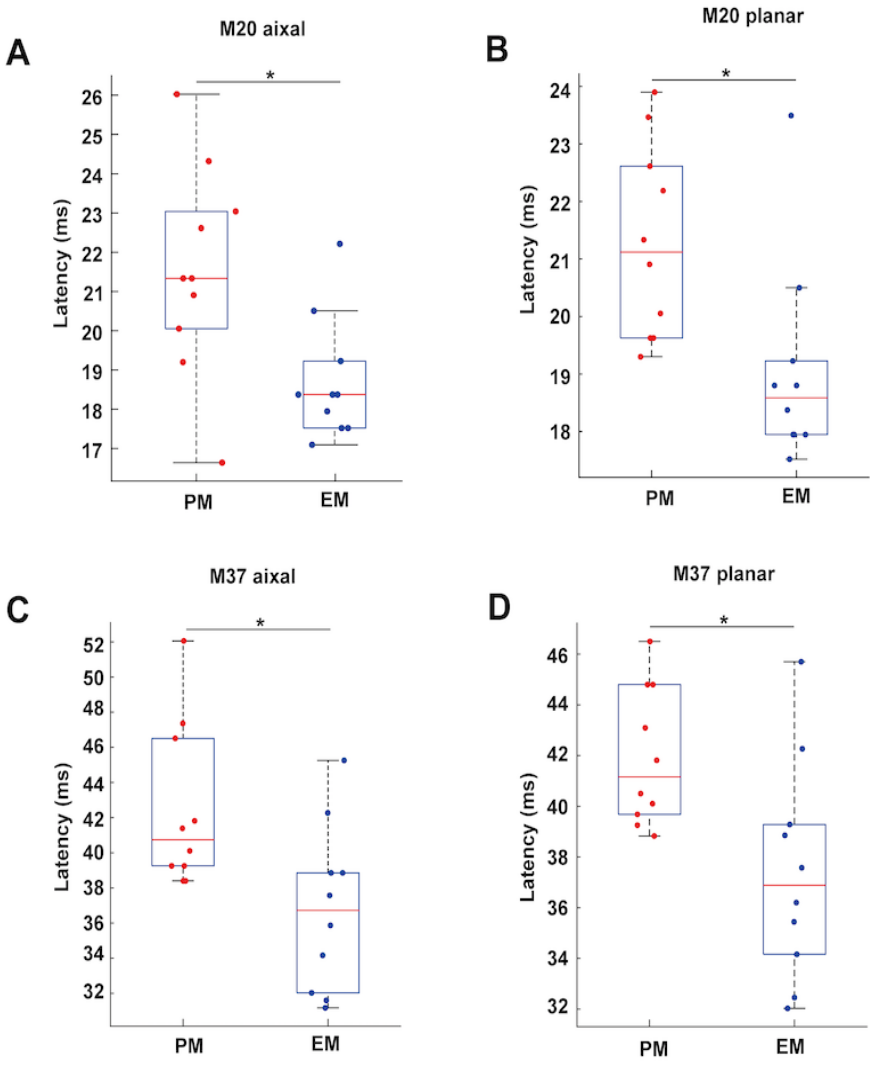

Figure 26. Latency differences of SEF components under electrical and pneumatic stimulation. (A and B) The bar graphs show a significant delay in M20 latency under pneumatic stimulation compared to electrical stimulation in axial and planar topographies (*P<0.05). (C and D) The comparison of M37 latencies shows a significant delay in pneumatic stimulation in axial and planar topographies (*P<0.05). *Indicates a statistically significant difference.

4 Discussion

4.1 The effects of stimulation type on M20 and M37 waveform characteristics

In this study, electrical stimulation yielded sharper waveforms with shorter latencies for M20 and M37 components. In contrast, pneumatic stimulation resulted in blurred or flat SEF waveforms, consistent with previous research findings(Antonakakis et al., 2019). The specific reasons for the differences in M20 and M37 waveforms between these two stimulation types are as follows:

1. **SNR Differences:**

   Electrical stimulation in general produces a significantly higher signal-to-noise ratio (SNR) compared to pneumatic stimulation, which results in clearer waveforms in somatosensory evoked potentials or fields. A higher SNR reduces the impact of background noise, allowing the true shape of the signal to be more easily observed. This clarity enhances the consistency of the waveforms across different trials, leading to sharper and more reliable average waveforms. Additionally, a higher SNR helps stabilize the timing of the waveforms, allowing for more accurate detection of neural responses(Leonardelli, 2010, Derzsi, 2021).

2. **Differences in Conduction Pathways:**

   The neural conduction pathways differ significantly between electrical and pneumatic stimulation, leading to variations in SEF waveform and latency. Electrical stimulation directly activates deep receptors or nerve endings, responsible for transmitting tactile and pressure sensations. This stimulation leads to rapid signal transmission to the spinal cord, thalamus, and primary somatosensory cortex (SI) (Nakamura et al., 1998). This conduction pathway produces faster and clearer neural response waveforms. In comparison, pneumatic stimulation activates mechanoreceptors, which are hindered by skin and surrounding tissue

interference, resulting in blurred SEF waveforms and slower propagation. slower propagation (Antonakakis et al., 2019).

Compared to pneumatic stimulation, electrical stimulation produces clearer, sharper, and more distinguishable SEF waveforms with higher SNR., making it highly suitable for clinical diagnostics. In contrast, while pneumatic stimulation elicits SEF waveforms that may appear blurred or flat, they resemble natural tactile responses, thereby remaining valuable for exploring somatosensory input and processing mechanisms.

4.2 The effects of stimulation type on M20 and M37 neural activation patterns

The effects of different stimulation types on the waveforms of SEF components M20 and M37 vary, yet the overall neural activation patterns remain highly similar. The cluster results indicated that after normalizing the stimulus intensity, there was no statistically significant difference in the activation amplitudes of M20 and M37 between electrical and pneumatic stimulation. Planar topographies revealed highly similar activation patterns for both M20 and M37 under both types of stimulation, likely due to their capability to accurately depict source signals and minimize noise effects(Niso Galán, 2013). However, the axial topography correlation for M37 disappeared after normalization, indicating that axial topography may be more sensitive to stimulation intensity. Thus, the conclusions based on planar topography are prioritized, further confirming the high similarity in neural activation patterns between the two stimulation types.

From a neurophysiological perspective, both electrical and pneumatic stimulation transmit somatosensory information to the primary somatosensory cortex (SI), which processes cortical somatosensory input. Regardless of stimulation type, the neural activation patterns generated in SI are similar. This consistency in

neuronal activation suggests that electrical and pneumatic stimulation may share common neural generators.Previous studies have shown that electrical and pneumatic stimulation can evoke similar sensory-evoked SI responses, but stimulus intensity's influence has often been overlooked (Nakamura et al., 1998). Our study demonstrated that electrical and pneumatic stimulation elicited comparable neural responses in the M20 and M37 components after normalizing stimulus intensity.

This study investigates how electrical and pneumatic stimulation influences the neural patterns of SEF components M20 and M37. Compared to axial topography, planar topography effectively illustrates these correlations, minimizing noise and accurately depicting neural activation patterns. Despite differing waveform characteristics, both stimulation methods evoke similar overall neural activation patterns.

4.3 The effects of normalized stimulus intensity on M20 and M37 neural activation patterns

To reduce the effects of stimulus intensity on neural responses, we compared the activation patterns of M20 and M37 under normalized and non-normalized stimulus conditions. In the non-normalized condition, cluster analyses showed that M20 under electrical stimulation exhibited higher amplitude than under pneumatic stimulation. Similarly, the planar topography of M37 presented comparable results. However, when stimulus intensity was normalized, the difference in activation amplitude between electrical and pneumatic stimuli disappeared. Under non-normalized stimulus intensity conditions, the correlation between M20 and M37 responses for electrical and pneumatic stimulation was higher, while this correlation significantly decreased under normalized conditions.Previous studies have consistently demonstrated a positive correlation between stimulus intensity and SEF, indicating that stronger stimulation elicits

greater SEF responses(Gatica Tossi et al., 2013, Jousmaki et al., 1998). For instance, the study by Mario A. Gatica Tossi et al. (2013) found that as stimulus intensity increased, the SEF response of the median nerve also enhanced. In comparison to their findings, although our experiment did not directly quantify changes in stimulus intensity, the differences in intensity between electrical and pneumatic stimulation may indeed influence neural responses. In the non-normalized condition, neuronal responses showed stronger positive correlations, reflecting the direct relationship between stimulus intensity and neural response strength across different stimulus types. However, normalizing stimulus strength attenuated this positive relationship, highlighting the fundamental correlation between stimulus types in how they modulate neural activity.

On the other hand, cluster and correlation analyses showed that statistical differences or correlations between electrical and pneumatic stimulation were reduced after normalization. This reduction may be because normalization did not improve the signal-to-noise ratio but amplified signals and noise equally. The high noise level associated with pneumatic stimulation may have impacted the statistical analysis, resulting in no significant differences.

Thus, this study demonstrates that stimulus intensity is a key factor influencing the correlations and differences in neural responses. Under non-normalized conditions, the activation patterns for both stimulus types were more similar despite differences in amplitude. Once the stimulus intensity was normalized, reducing the effect of intensity, it became evident that the two stimulus types were intrinsically correlated in neural responses, with no significant differences in amplitude. Nevertheless, the noise in the pneumatic condition could obscure these differences, and the remaining high correlation indicates a correlation in topographies even after normalization.

5 Summary

Somatosensory evoked fields (SEFs) can be recorded following either electrical or mechanical stimulation, allowing for the investigation of brain responses to different somatosensory pathways. This study compares SEF components elicited by electrical and pneumatic stimulation to assess whether pneumatic stimulation could serve as an alternative to electrical stimulation, particularly for reducing patient discomfort. Recordings of the M20 and M37 components were obtained from 10 subjects under both types of stimulation. The analysis focused on signal-to-noise ratio (SNR), SEF waveform characteristics, topographical differences, and correlations.

The results demonstrated that: (1) Electrical stimulation produced clearer SEF waveforms, shorter latencies, and higher SNR compared to pneumatic stimulation; (2) After normalizing stimulus intensity, the topographies of M20 and M37 components were highly correlated between electrical and pneumatic stimulation.

In conclusion, while electrical stimulation remains the preferred method in clinical settings due to its superior SNR, clearer SEF waveforms, and shorter latencies, pneumatic stimulation offers potential as a research tool in neuroscience, particularly for exploring natural tactile mechanisms and minimizing subject discomfort.

Zusammenfassung

Somatosensorisch evozierte Felder (SEF) können sowohl nach elektrischer als auch nach mechanischer Stimulation aufgezeichnet werden, was die Untersuchung der Gehirnantwort auf unterschiedliche somatosensorische Bahnen ermöglicht. Diese Studie vergleicht SEF-Komponenten, die durch

elektrische und pneumatische Stimulation ausgelöst werden, um zu prüfen, ob pneumatische Stimulation als Alternative zur elektrischen Stimulation dienen kann, insbesondere zur Reduzierung von Patientenbeschwerden. Aufzeichnungen der M20- und M37-Komponenten wurden bei 10 Probanden unter beiden Stimulationsarten durchgeführt. Die Analyse konzentrierte sich auf das Signal-Rausch-Verhältnis (SNR), die Charakteristika der SEF-Wellenformen, topographische Unterschiede und Korrelationen.

Die Ergebnisse zeigten: (1) Elektrische Stimulation erzeugte im Vergleich zur pneumatischen Stimulation klarere SEF-Wellenformen, kürzere Latenzen und ein höheres SNR; (2) Nach der Normalisierung der Stimulusintensität waren die Topographien der M20- und M37-Komponenten zwischen elektrischer und pneumatischer Stimulation hoch korreliert.

Zusammenfassend bleibt die elektrische Stimulation aufgrund ihres überlegenen SNR, der klareren SEF-Wellenformen und der kürzeren Latenzen die bevorzugte Methode in klinischen Anwendungen. Die pneumatische Stimulation zeigt jedoch Potenzial als Forschungsinstrument in der Neurowissenschaft, insbesondere zur Untersuchung natürlicher taktiler Mechanismen und zur Minimierung von Patientenbeschwerden.

6 Reference

Abraira, V. E. & Ginty, D. D. 2013. The sensory neurons of touch. *Neuron,* 79**,** 618-639.

Antonakakis, M., Schrader, S., Wollbrink, A., Oostenveld, R., Rampp, S., Haueisen, J. & Wolters, C. H. 2019. The effect of stimulation type, head modeling, and combined eeg and meg on the source reconstruction of the somatosensory p20/n20 component. *Hum Brain Mapp,* 40**,** 5011-5028.

Anzellotti, F., Onofrj, M., Bonanni, L., Saracino, A. & Franciotti, R. 2016. Giant early components of somatosensory evoked potentials to tibial nerve stimulation in cortical myoclonus. *Neuroimage Clin,* 12**,** 212-218.

Assenza, G., Lanzone, J., Dubbioso, R., Coppola, A., Boscarino, M., Ricci, L., Insola, A., Bilo, L., Tombini, M. & Di Lazzaro, V. 2020. Thalamic and cortical hyperexcitability in juvenile myoclonic epilepsy. *Clin Neurophysiol,* 131**,** 2041-2046.

Babiloni, C., Pizzella, V., Gratta, C. D., Ferretti, A. & Romani, G. L. 2009. Fundamentals of electroencefalography, magnetoencefalography, and functional magnetic resonance imaging. *Int Rev Neurobiol,* 86**,** 67-80.

Baillet, S. 2017. Magnetoencephalography for brain electrophysiology and imaging. *Nat Neurosci,* 20**,** 327-339.

Beppi, C., Ribeiro Violante, I., Scott, G. & Sandrone, S. 2021. Eeg, meg and neuromodulatory approaches to explore cognition: Current status and future directions. *Brain Cogn,* 148**,** 105677.

Bromm, B. & Lorenz, J. 1998. Neurophysiological evaluation of pain. *Electroencephalogr Clin Neurophysiol,* 107**,** 227-253.

Buchner, H., Fuchs, M., Wischmann, H. A., Dossel, O., Ludwig, I., Knepper, A. & Berg, P. 1994. Source analysis of median nerve and finger stimulated somatosensory evoked potentials: Multichannel simultaneous recording of electric and magnetic fields combined with 3d-mr tomography. *Brain Topogr,* 6**,** 299-310.

Cargnelutti, E. & Tomasino, B. 2023. Pre-operative functional mapping in patients with brain tumors by fmri and meg: Advantages and disadvantages in the use of one technique over the other. *Life (Basel),* 13.

Cohen, D. 1968. Magnetoencephalography: Evidence of magnetic fields produced by alpha-rhythm currents. *Science,* 161**,** 784-786.

Cohen, D. 1972. Magnetoencephalography: Detection of the brain's electrical activity with a superconducting magnetometer. *Science,* 175**,** 664-666.

Cruccu, G., Aminoff, M. J., Curio, G., Guerit, J. M., Kakigi, R., Mauguiere, F., Rossini, P. M., Treede, R. D. & Garcia-Larrea, L. 2008. Recommendations for the clinical use of somatosensory-evoked potentials. *Clin Neurophysiol,* 119**,** 1705-1719.

Derzsi, Z. 2021. Optimal approach for signal detection in steady-state visual evoked potentials in humans using single-channel eeg and stereoscopic

stimuli. *Frontiers in Neuroscience,* 15**,** 600543.
Faley, M., Poppe, U., Urban, K., Paulson, D. & Fagaly, R. A new generation of the hts multilayer dc-squid magnetometers and gradiometers. Journal of physics: conference series, 2006. IOP Publishing, 1199.
Fred, A. L., Kumar, S. N., Kumar Haridhas, A., Ghosh, S., Purushothaman Bhuvana, H., Sim, W. K. J., Vimalan, V., Givo, F. A. S., Jousmaki, V., Padmanabhan, P. & Gulyas, B. 2022. A brief introduction to magnetoencephalography (meg) and its clinical applications. *Brain Sci,* 12.
Gatica Tossi, M. A., Lillemeier, A. S. & Dinse, H. R. 2013. Influence of stimulation intensity on paired-pulse suppression of human median nerve somatosensory evoked potentials. *Neuroreport,* 24**,** 451-456.
Hämäläinen, M., Hari, R., Ilmoniemi, R. J., Knuutila, J. & Lounasmaa, O. V. 1993. Magnetoencephalography—theory, instrumentation, and applications to noninvasive studies of the working human brain. *Reviews of modern Physics,* 65**,** 413.
Hämäläinen, M. S. & Ilmoniemi, R. J. 1994. Interpreting magnetic fields of the brain: Minimum norm estimates. *Medical & biological engineering & computing,* 32**,** 35-42.
Hari, R., Reinikainen, K., Kaukoranta, E., Hamalainen, M., Ilmoniemi, R., Penttinen, A., Salminen, J. & Teszner, D. 1984. Somatosensory evoked cerebral magnetic fields from si and sii in man. *Electroencephalogr Clin Neurophysiol,* 57**,** 254-263.
Henry, J. C. 2006. Electroencephalography: Basic principles, clinical applications, and related fields. *Neurology,* 67**,** 2092-2092-a.
Hitomi, T., Ikeda, A., Matsumoto, R., Kinoshita, M., Taki, J., Usui, K., Mikuni, N., Nagamine, T., Hashimoto, N., Shibasaki, H. & Takahashi, R. 2006. Generators and temporal succession of giant somatosensory evoked potentials in cortical reflex myoclonus: Epicortical recording from sensorimotor cortex. *Clin Neurophysiol,* 117**,** 1481-1486.
Holmes, N., Rea, M., Chalmers, J., Leggett, J., Edwards, L. J., Nell, P., Pink, S., Patel, P., Wood, J., Murby, N., Woolger, D., Dawson, E., Mariani, C., Tierney, T. M., Mellor, S., O'Neill, G. C., Boto, E., Hill, R. M., Shah, V., Osborne, J., Pardington, R., Fierlinger, P., Barnes, G. R., Glover, P., Brookes, M. J. & Bowtell, R. 2022. A lightweight magnetically shielded room with active shielding. *Sci Rep,* 12**,** 13561.
Jousmaki, V. & Forss, N. 1998. Effects of stimulus intensity on signals from human somatosensory cortices. *Neuroreport,* 9**,** 3427-3431.
Kaas, J. H. 2004. Somatosensory system. *The human nervous system***,** 1059-1092.
Kakigi, R., Koyama, S., Hoshiyama, M., Shimojo, M., Kitamura, Y. & Watanabe, S. 1995. Topography of somatosensory evoked magnetic fields following posterior tibial nerve stimulation. *Electroencephalogr Clin Neurophysiol,* 95**,** 127-134.

Kallio, M. 2018. *Activity in somatosensory cortices during stroke recovery.*
Kallmann, B. A., Fackelmann, S., Toyka, K. V., Rieckmann, P. & Reiners, K. 2006. Early abnormalities of evoked potentials and future disability in patients with multiple sclerosis. *Mult Scler,* 12**,** 58-65.
Leonardelli, E. 2010. A multimodal neuroimaging study of somatosensory system.
Levin, K. H. & Chauvel, P. 2019. *Clinical neurophysiology: Basis and technical aspects: Handbook of clinical neurology series*, Elsevier.
Lew, S., Wolters, C. H., Anwander, A., Makeig, S. & MacLeod, R. S. 2009. Improved eeg source analysis using low-resolution conductivity estimation in a four-compartment finite element head model. *Hum Brain Mapp,* 30**,** 2862-2878.
Maudrich, T., Hahner, S., Kenville, R. & Ragert, P. 2021. Somatosensory-evoked potentials as a marker of functional neuroplasticity in athletes: A systematic review. *Front Physiol,* 12**,** 821605.
McCarthy, G. & Wood, C. C. 1985. Scalp distributions of event-related potentials: An ambiguity associated with analysis of variance models. *Electroencephalography and Clinical Neurophysiology/Evoked Potentials Section,* 62**,** 203-208.
Mertens, M. & Lutkenhoner, B. 2000. Efficient neuromagnetic determination of landmarks in the somatosensory cortex. *Clin Neurophysiol,* 111**,** 1478-1487.
Meyer, S. S. 2016. *Source modelling of the human hippocampus for meg.* UCL (University College London).
Michel, C. M., Murray, M. M., Lantz, G., Gonzalez, S., Spinelli, L. & De Peralta, R. G. 2004. Eeg source imaging. *Clinical neurophysiology,* 115**,** 2195-2222.
Nakamura, A., Yamada, T., Goto, A., Kato, T., Ito, K., Abe, Y., Kachi, T. & Kakigi, R. 1998. Somatosensory homunculus as drawn by meg. *Neuroimage,* 7**,** 377-386.
Niso Galán, J. G. 2013. *Functional and effective connectivity in meg. Application to the study of epilepsy.* Telecomunicacion.
Onishi, H., Sugawara, K., Yamashiro, K., Sato, D., Suzuki, M., Kirimoto, H., Tamaki, H., Murakami, H. & Kameyama, S. 2013. Effect of the number of pins and inter-pin distance on somatosensory evoked magnetic fields following mechanical tactile stimulation. *Brain Res,* 1535**,** 78-88.
Ostry, S., Nevsimal, M., Nevsimalova, M., Reiser, M. & Fiedler, J. 2021. Median somatosensory evoked potential as a predictor of clinical outcome after urgent surgical extracranial internal carotid artery recanalization. *Clin Neurophysiol,* 132**,** 372-381.
Pakkenberg, B., Pelvig, D., Marner, L., Bundgaard, M. J., Gundersen, H. J., Nyengaard, J. R. & Regeur, L. 2003. Aging and the human neocortex. *Exp Gerontol,* 38**,** 95-99.
Purves, D. 2018. *Neuroscience,* New York, Oxford University Press.
Purves, D., Augustine, G. J., Fitzpatrick, D., Hall, W., LaMantia, A.-S. & White, L.

2019. *Neurosciences*, De Boeck Supérieur.
Tecchio, F., Zappasodi, F., Tombini, M., Caulo, M., Vernieri, F. & Rossini, P. M. 2007. Interhemispheric asymmetry of primary hand representation and recovery after stroke: A meg study. *Neuroimage,* 36**,** 1057-1064.
Torebjork, H. E. & Ochoa, J. L. 1980. Specific sensations evoked by activity in single identified sensory units in man. *Acta Physiol Scand,* 110**,** 445-447.
van Mierlo, P., Holler, Y., Focke, N. K. & Vulliemoz, S. 2019. Network perspectives on epilepsy using eeg/meg source connectivity. *Front Neurol,* 10**,** 721.
Vrba, J. 2002. Magnetoencephalography: The art of finding a needle in a haystack. *Physica C: Superconductivity,* 368**,** 1-9.
Vrba, J. & Robinson, S. E. 2001. Signal processing in magnetoencephalography. *Methods,* 25**,** 249-271.
Walsh, P., Kane, N. & Butler, S. 2005. The clinical role of evoked potentials. *J Neurol Neurosurg Psychiatry,* 76 Suppl 2**,** ii16-22.
Wang, L., Jensen, O., van den Brink, D., Weder, N., Schoffelen, J. M., Magyari, L., Hagoort, P. & Bastiaansen, M. 2012. Beta oscillations relate to the n400m during language comprehension. *Hum Brain Mapp,* 33**,** 2898-2912.
Williamson, S. J., Romani, G.-L., Kaufman, L. & Modena, I. 2013. *Biomagnetism: An interdisciplinary approach*, Springer Science & Business Media.
Zhu, K. & Kiourti, A. 2022. A review of magnetic field emissions from the human body: Sources, sensors, and uses. *IEEE Open Journal of Antennas and Propagation,* 3**,** 732-744.

7 Declaration of contributions

This dissertation is the result of collaborative work involving several contributors, whose efforts I acknowledge here. The following declaration outlines the specific contributions made by me and others to the design, data collection, analysis, supervision, and writing of this work.

Study Design

The work was conducted at the MEG Center of the University Hospital of Tübingen under the supervision of PD Dr. Justus Marquetand.

The overall study design was conceptualized by myself, in consultation with my supervisor, PD Dr. Justus Marquetand.I carried out the experiments independently, following comprehensive training provided by PD Dr. Justus Marquetand.

Data Collection and Experiments

I personally carried out the majority of the experimental work presented in this dissertation, including:

1) All MEG recordings of participants.

Data Analysis and Statistical Work

I performed the primary statistical analysis of the data, including:

1) MEG data preprocessing.

2) The statistical analysis of the experimental data was performed personally, with guidance from Hui Chen.

3) Visualization of the results.

Writing and Publication

I wrote the dissertation independently, including drafting and revising the manuscript. PD. Dr. Justus Marquetand provided editorial suggestions, helping to refine the text and improve the clarity of scientific arguments. Prof. Dr. Christoph Braun provided valuable suggestions for revising the methodology section.

Acknowledgement of Other Contributions

I would like to acknowledge Mr. Jürgen Dax for his technical in equipment troubleshooting, which was essential to the completion of this work.

In conclusion, while this dissertation is a collaborative effort, the majority of the intellectual and practical contributions, including study design, data collection, analysis, and writing, were made by me, with significant guidance from my supervisors and collaborators as mentioned above.

_____

Place / date / signature of doctoral candidate

8 Acknowledgments

I express my gratitude to all participants of this study, whose contributions are essential.

Many thanks to my supervisor, PD Dr. Justus Marquetand, for his guidance and for providing the opportunity to engage deeply with medical research.

I thank my colleagues at the MEG Center for their support and the China Scholarship Council (CSC) for financially supporting my doctoral study in Europe.

Finally, I extend my heartfelt thanks to my parents, Hui Chen, family, and friends in China for their unwavering support throughout my journey in Germany.